CWENO reconstructions for balance laws

I. Cravero, G. Puppo, M. Semplice, G. Visconti

Abstract In this paper we introduce a general framework for defining and studying essentially non-oscillatory reconstruction procedures of arbitrarily high order accuracy, interpolating data in a central stencil around a given computational cell (CWENO). This technique relies on the same selection mechanism of smooth stencils adopted in WENO, but the pool of candidates for the selection includes polynomials of different degrees. This seemingly minor difference allows to compute an analytical expression of a polynomial interpolant, approximating the unknown function uniformly within a cell, instead of just selected points. For this reason this technique is particularly suited for balance laws for finite volume schemes, when averages of source terms require high order quadrature rules based on several points; in the computation of local averages, during refinement in h-adative schemes; or in the initialization of a timestep in moving mesh techniques, and in general when a globally defined reconstruction is needed. Previously, these needs were satisfied by ENO reconstruction techniques, which, however, require a much wider stencil then the CWENO reconstruction studied here, for the same accuracy.

Keywords high order accuracy, essentially non oscillatory, finite volume schemes, balance laws, non uniform grids.

1 Introduction

Motivation. Conservation laws arise in many fields in applied mathematics, such as gas dynamics or magnetohydrodynamics, or even traffic flow. When a source term is present, these equations are called balance laws, and even a wider field of applications opens up. Balance laws describe in fact phenomena in environmental or metheorological fields, plasmas, astrophysics.

In many cases, fast and efficient algorithms are crucial, and this means to be able to provide robust high order schemes, which yield accurate solutions even on coarse grids. Moreover, it is important to be able to implement such schemes on adaptive, and therefore non uniform, grids. This paper is concerned with the analysis of a class of algorithms which starting from a set of data permit to reconstruct with high order accuracy a representation in space of the underlying function.

We start from a standard balance law

$$\partial_t u + \sum_{i=1}^{n} \partial_{x_i} f_i(u) = s(u;x). \tag{1}$$

In this system of equations $u(x,t) : \mathbb{R}^n \times \mathbb{R}^+ \to \mathbb{R}^m$ is the unknown function, n is the number of space dimensions, m is the number of equations, and t denotes time. The functions $f_i(u) : \mathbb{R}^m \to \mathbb{R}^m$ are called fluxes, and usually they are smooth known functions of u, with Jacobians $\sum_i \omega_i f_i'$ diagonalizable with real eigenvalues, along all possible directions $\omega \in \mathbb{R}^n$. Finally, $s : \mathbb{R}^m \times \mathbb{R}^n$ is the source term, which is a known, bounded function of the unknown u, but also it may depend on space (as in the shallow water equations), or even time. Suppose the equation is defined on a domain $\mathcal{D} \in \mathbb{R}^n$, with suitable initial and boundary conditions.

To integrate this system of equations numerically, one must define a *grid* in the domain $\mathcal{D}$. In this work, we will propose schemes that are of interest in particular when the grid is a non uniform cartesian grid, so that $\mathcal{D}$ is covered with the union of rectangles $\mathcal{D} \in \bigcup \Omega_k$. Boundary conditions can then be dealt with immersed boundary techniques, see [SCR16] or [GITW12].

On each cell Ω_k, define the *cell average* of the solution,

$$\overline{u}_k(t) = \frac{1}{\mu(\Omega_k)} \int_{\Omega_k} u(x,t)\, \mathrm{d}x. \tag{2}$$

Using the method of lines, we integrate the balance law (1) on each of the Ω_k, obtaining the finite volume formulation

$$\frac{\mathrm{d}}{\mathrm{d}t}\overline{u}_k = -\frac{1}{\Omega_k} \int_{\partial\Omega_k} \mathbf{f} \cdot \mathbf{n}_k + \frac{1}{\Omega_k} \int_{\Omega_k} s(u;x)\, \mathrm{d}x, \tag{3}$$

where $\mathbf{f} = [f_1, \ldots, f_n]$ and $\mathbf{n}_k$ is the outward normal to the cell Ω_k. To transform (3) in a Finite Volume numerical scheme, a recipe for the evaluation of the fluxes across the cell boundary must be provided, together with a numerical method to integrate the resulting system of ODE's. But another key point is the fact that a *reconstruction* algorithm must be provided, which, starting from the cell averages at a given time t, reconstructs approximate values of the solution u in all the quadrature points along the contour $\partial\Omega_k$ of each cell to evaluate the numerical fluxes, and in all quadrature nodes within Ω_k, to reconstruct the cell average of the source. The purpose of the present work is to study a class of reconstructions which provide an approximation of the underlying solution which is *uniformly* accurate within the whole cell. In this fashion, the reconstruction can be evaluated simultaneously on all quadrature points needed to approximate (3), thus only one reconstruction step is needed for each evaluation of the right hand side.

Background. A very popular algorithm to compute the reconstruction in high order FV schemes for conservation and balance laws is WENO (Weighted

Essentially Non Oscillatory), see the seminal paper [JS96] and the reviews [Shu98, Shu09], but the literature on this technique is huge. WENO is based on the computation of a piecewise polynomial reconstruction, which reproduces a high order polynomial in regions of smoothness (thus providing high accuracy), using data from a wide stencil, which degrades automatically to lower order polynomials, when a discontinuity is detected within the large stencil. The lower order polynomials are based on smaller stencils, chosen in order to avoid the discontinuity. High accuracy is obtained blending the lower order polynomials together, with carefully designed non linear weights, which reproduce the value that would be given, at one particular point, by the high order polynomial that would interpolate the data on the wide stencil. Since the high order optimal polynomial is actually never computed, its values are replicated only at one or two points, by an ad hoc combination of the low order polynomials. If the reconstruction is needed at several points, as in the quadratures required by the integration of (3), then several reconstruction steps must be computed, each time with different weights.

This problem is particularly severe in balance laws, such as the shallow water equation, where one needs to evaluate the source at quadrature points in the interior of the cell. In fact, for WENO 3 optimal weights for the cell center do not exist and for WENO 5 they exist but are not in $[0, 1]$. There is a technique to treat negative weights [SHS02], but it requires to compute two different reconstructions per point. Also, the evaluation of a posteriori error indicators may require to compute accurate quadratures of some form of the local residual, as in the the case of the indicator based on the entropy production, see [Pup04, PS11, PS16]. Again, the possibility of computing the reconstruction at interior nodes is crucial.

Moreover, in non-uniform grids, WENO weights depend on the mesh geometry. For example, in 1D, the weights depend on the ratio of the sizes of the neighbour and of the current cell, see e.g. [WFS08, PS16], and they additionally also depend on the disposition of the neighboring cells in 2D [HS99, DK07, PS14].

A source of non uniform grids typically is mesh adaptivity of h-type or moving mesh algorithms. Both these techniques need the spatial reconstruction for time advancement, but also to perform another important task. In fact, they both involve a change in the mesh that occours after the conclusion of each time step. In these cases, it is necessary to project the solution from one grid to the new mesh produced by the adaptive algorithm. The cells of the new grid are subcells of the previous ones in the case of h-AMR ([CRS16, KPL13]) while they lie in more general positions in the case of moving mesh methods (see e.g.[TT03]). For schemes of order at least 3, one must be able to compute the subcell averages with the same accuracy of the scheme and this requires quadrature formulas and thus reconstructions at inner points, see e.g. [CRS16].

Other schemes for which this reconstructions can be of interest are the $\mathrm{P_N P_M}$ schemes of [DBTM08] in which at each step a reconstruction from cell averages is required to compute a reliable polynomial reconstruction inside each cell. Here one needs the functional expression of the polynomial and not just its point values.

Summary. The first instance in which the need to have an expression for the reconstruction polynomial was answered, was in the construction of a third order central scheme in [LPR99]. There the authors introduced a new reconstruction procedure of order three. In this paper we extend this idea to a general technique to obtain a high order, essentially non-oscillatory, interpolation polynomial that is globally defined in the whole cell. (§3).

The new reconstructions are based on an optimal polynomial defined on a central large stencil and on a set of lower degree polynomials defined on sub-stencils of the bigger one. The selection mechanisms of the polynomials actually employed to compute the reconstruction is similar to the WENO one (reviewed in §2), but it includes an extra polynomial of the same degree of the optimal one. For this reason we call the reconstructions Central WENO (CWENO). The main difference between WENO and CWENO is that the latter does not compute reconstructed values at given points in the cell but rather a reconstruction polynomial defined in the whole cell.

The convergence rates of the CWENO reconstructions, when the Jiang-Shu smoothness indicators of [JS96] are employed, depends on the value chosen for the small parameter ϵ appearing in the algorithm. This value must be chosen according to the behaviour of the smoothness indicators close to local extrema and is thus present in the WENO setting as well. Many techniques were proposed to overcome this difficulty in the WENO framework, [HAP05, FHW14, DB13, ABBM11]. The technique of [ABBM11], consisting in choosing a value for ϵ as a function of the mesh size, was extended to the CWENO setting, at order 3, by [Kol14] on uniform grids and by [CS] on a non-uniform mesh. In §4 we show that the choices $\epsilon \sim h^2$ and $\epsilon \sim h$ guarantee the optimal convergence rate for a CWENO construction of any order, under the mild condition that no polynomial involved in the reconstruction is of degree smaller than one half of the desired accuracy on smooth solutions.

The essentially non-oscillatory behaviour of CWENO when the data to be interpolated contain a discontinuity is, from a practical point of view, very similar to that of WENO. However, from a theoretical point of view, the situation is quite different, due to the employment of the extra candidate polynomial of high degree. In §5 we introduce a condition (that we call *Property R*) that must be satisfied by this extra high degree candidate polynomial in order to ensure that the reconstruction has essentially non-oscillatory properties. Furthermore, we show that this property is satisfied by all the CWENO constructions of order 3,5, and 7 we introduce, under mild conditions on the choice of the linear weights.

Finally, in §6 we provide extensive numerical evidence of the accuracy and non-oscillatory behaviour of CWENO constructions of order up to 9. Furthermore, in order to test the reconstruction at points in the interior of the computational cells, we show applications to the Euler gas dynamics equation with source terms and to the development of well-balanced schemes for the shallow water equation.

2 WENO revisited

Fixing a stencil $\{\Omega_{j-g}, \dots, \Omega_{j+g}\}$, the definition of $P_{\mathsf{rec},j}$ that maximises the accuracy for smooth functions $u(x)$ is clearly the polynomial P_{opt} of degree $G = 2g$ which interpolates the $2g+1$ cell averages $\overline{u}_{j-g}, \dots, \overline{u}_{j+g}$, which is easily computed following [Shu98]. Obviously, such a polynomial might be very oscillatory if a jump discontinuity is present in the stencil. In this case, WENO makes use of polynomials of lower degree (g) whose stencils avoids the discontinuity.

Definition 1. *Fix a point $\hat{x} \in \Omega_j$ and an integer g. The* WENO *reconstruction operator is given by*

$$P_{\mathsf{rec},j}(\hat{x}) = \mathsf{WENO}(P_1, \dots, P_{g+1}; P_{\mathsf{opt}}, \hat{x}) \in \mathbb{R},$$

where the P_k's, $k = 1, \dots, g+1$ are polynomials of degree g, P_{opt} is a polynomial of degree $G = 2g$ which guarantees the required accuracy $2g+1$, and is computed as follows:

1. *First, find a set of coefficients $d_1(\hat{x}), \dots, d_{g+1}(\hat{x})$ such that*

$$\sum_{k=1}^{g+1} d_k(\hat{x}) P_k(\hat{x}) = P_{\mathsf{opt}}(\hat{x}) \quad \text{and} \quad \sum_{k=1}^{g+1} d_k(\hat{x}) = 1.$$

   These will be called optimal or linear coefficients.

2. *Then nonlinear coefficients ω_k are computed from the optimal (or linear) ones as*

$$\alpha_k = \frac{d_k}{(I[P_k] + \epsilon)^t} \qquad \omega_k = \frac{\alpha_k}{\sum_{k=1}^{g+1} \alpha_k}, \tag{4}$$

   where $I[P_k]$ denotes a suitable regularity indicator (to be defined later) evaluated on the polynomial P_k, ϵ is a small positive quantity and $t \geq 2$.

3. *Finally*

$$P_{\mathsf{rec},j}(\hat{x}) = \sum_{k=1}^{g+1} \omega_k P_k(\hat{x}) \tag{5}$$

The regularity indicators should measure the "smoothness" of the polynomial P_k on the computational cell Ω_j. A regularity indicator is a positive semidefinite operator from $\mathbb{P}$ to $\mathbb{R}^+$, which typically depends on the derivatives of the polynomial as a way to detect its oscillatory behaviour. The classical example is the Jiang-Shu indicator, defined in [JS96] as

$$I[P] = \sum_{l \geq 1} \mathrm{diam}(\Omega)^{2l-1} \int_\Omega [P^{(l)}(x)]^2 \mathrm{d}x \tag{6}$$

Note that the summation is in fact finite, and that on smooth data $I[P] = \mathcal{O}(\mathrm{diam}(\Omega))^2$ at most. In this work we will employ the Jiang-Shu indicators, but other possibilities were explored in [**?**, **?**] . We record here an useful property of these indicators.

Complete these references, and check the $\mathcal{O}$ qui sopra

Remark 1. *The Jiang-Shu indicator of a polynomial P is Lipschitz continuous with respect to the cell averages $\overline{u}_{j-r}, \dots, \overline{u}_{j+s}$, with r and s positive integers, interpolated by P. In fact, P depends linearly on the data and thus I_P is a positive semidefinite quadratic form with respect to $\overline{u}_{j-r}, \dots, \overline{u}_{j+s}$.*

Summary 1. *The ingredients of the success of the* WENO *reconstruction are the following.*

1. *The regularity indicators* (6) *which are of size $\mathcal{O}(h^2)$ on regular data, but $I[P] \asymp 1$ in the case of discontinuous data, where with $\asymp 1$ we mean "of the same order of 1, and bounded away from zero".*

2. *Thanks to the definition of the nonlinear weights, the reconstruction error at point $\hat{x}$ is given by*

$$\begin{aligned} u(\hat{x}) - P_{\mathsf{rec},j}(\hat{x}) &= u(\hat{x}) - P_{\mathsf{opt}}(\hat{x}) + \sum_k \big(d_k(\hat{x}) - \omega_k(\hat{x})\big) P_k(\hat{x}) \\ &= \underbrace{\big(u(\hat{x}) - P_{\mathsf{opt}}(\hat{x})\big)}_{\mathcal{O}(h^{2g+1})} + \sum_k \big(d_k(\hat{x}) - \omega_k(\hat{x})\big) \underbrace{\big(P_k(\hat{x}) - u(\hat{x})\big)}_{\mathcal{O}(h^{g+1})} \end{aligned} \tag{7}$$

   where the last equality is true since $\sum_k d_k = \sum_k \omega_k = 1$. From the above formula it is clear that the accuracy of the WENO *reconstruction equals the accuracy of its first argument P_{opt} only if $d_k - \omega_k = \mathcal{O}(h^g)$ in the case of smooth data. This is ensured by the regularity of the smoothness indicators and by an appropriate choice of the parameter ϵ (see [ABBM11, CS]).*

3. *In the case of discontinous data, suppose that there is one smooth substencil, so that at least one of the regularity indicators is $\mathcal{O}(h^2)$. Then, the renormalization procedure in* (4) *ensures that for all k such that $I[P_k] \asymp 1$, then $\omega_k \simeq 0$. In this way, only the P_k's with $I[P_k] = \mathcal{O}(h^2)$ contribute to the reconstruction. This is the case provided there is one singularity in the stencil, which does not occour in the central cell.*

4. *On the other hand, if the discontinuity is in the central cell, each $I[P_k] \asymp 1$. In the case of finite differences (see [Shu98, HOEC86]) one can prove that each candidate polynomial is monotone in the central cell and thus deduce that the reconstructed value will not increase the total variation. In the case of finite volumes, instead, the reconstructed data is not guaranteed to satisfy TVD bounds, although typically spurious oscillations are not observed.*

For example, for reconstructions from point values applied to the case of Heaviside data, all candidate polynomials are bounded by the values before and after the jump, see [Shu98, p. 347]. The reconstruction is then total variation bounded for the case of Heaviside data with a Lispshitz perturbation, see [HOEC86, Theor 4.1, p. 359].

This procedure is nevertheless extremely successfull and allowed to construct very high order essentially non-oscillatory schemes (see [Shu09] and references therein), but it has a few shortcomings. The linear coefficients $d_k(\hat{x})$ depend explicitly on the location of $\hat{x}$ inside the cell Ω_j. (Their values have been tabulated for the cell boundaries in one space dimension for uniform grids [Shu98, ABBM11]). In order to construct a finite volume scheme, the computation of linear and nonlinear weights is required at different points on the cell boundary: two points in one space dimension and at least six (on triangles) and 8 on a Cartesian mesh for a scheme of oder at least three in two space dimensions. Even more reconstructions are needed for balance laws, where the cell average of the source has to be evaluated, and for higher dimensions.

Moreover, for interior points, the linear coefficients may not exist (e.g. WENO3 at cell center) or be non-positive (e.g. WENO5 at cell center). Results on the existence of $d_k(\hat{x})$ for general $\hat{x}$ have been proven for example in [CFR06, Ger12]. A procedure to circumvent the appearance of negative weights was proposed in [SHS02].

From the next section, we study the CWENO schemes which are not affected by any of these troubles, since the linear coefficients are not needed to guarantee the accuracy of the reconstruction in smooth cases. Thus they can be chosen rather arbitrarily and be the same for every reconstruction point in the cell. An additional advantage is that the computation of the α_k and the ω_k is performed only once per cell and not once per reconstruction point.

3 The CWENO operator

In this section we introduce a general setting for introducing the CWENO reconstruction, which encompasses the one of [LPR99] and all variations published later in one and more space dimensions, on structured and unstructured grids. Moreover, this will allow us to propose higher order extensions.

Definition 2. *Consider a set of data (point values or cell averages) and a polynomial P_{opt} of degree G, which interpolates in some sense all the given data (*optimal polynomial*). The* CWENO *operator computes a reconstruction polynomial*

$$P_{\mathsf{rec}} = \mathsf{CWENO}(P_{\mathsf{opt}}, P_1, \ldots, P_{\widehat{m}}) \in \mathbb{P}^G$$

from $P_{\mathsf{opt}} \in \mathbb{P}^G$ and a set of lower order alternative polynomials $P_1, \ldots, P_{\widehat{m}} \in \mathbb{P}^g$, where $g < G$ and $\widehat{m} \geq 1$. The definition of P_{rec} depends on the choice of a set of positive real coefficients $d_0, \ldots, d_{\widehat{m}} \in [0,1]$ such that $\sum_{k=0}^{\widehat{m}} d_k = 1$ (called linear coefficients*) as follows:*

1. *first, introduce the polynomial P_0 defined as*

$$P_0(x) = \frac{1}{d_0}\left(P_{\mathsf{opt}}(x) - \sum_{k=1}^{\widehat{m}} d_k P_k(x)\right) \in \mathbb{P}^G \tag{8}$$

2. *then the nonlinear coefficients* ω_k *are computed from the linear ones as*

$$\alpha_k = \frac{d_k}{(I[P_k]+\epsilon)^t} \qquad \omega_k = \frac{\alpha_k}{\sum_{k=0}^{\widehat{m}} \alpha_k}, \tag{9}$$

where $I[P_k]$ *denotes a suitable regularity indicator (e.g. the Jiang-Shu ones of eq.* (6)*) evaluated on the polynomial* P_k*,* ϵ *is a small positive quantity and* $t \geq 2$*;*

3. *and finally*

$$P_{\mathsf{rec}}(x) = \sum_{k=0}^{\widehat{m}} \omega_k P_k(x) \in \mathbb{P}^G. \tag{10}$$

Note that the polynomial $P_0 \in \mathbb{P}^G$ *is* part of the reconstruction, which provides a polynomial that can be evaluated at any point within the cell, and all coefficients ω_k involved in the reconstruction *do not* depend on the particular points where the reconstruction is needed.

Remark 2. *In the case of reconstruction from cell averages, from the definition, it is trivial to check that, if all candidate polynomials satisfy the conservation property*

$$\tfrac{1}{|\Omega|}\int_\Omega P_{\mathsf{opt}}\mathrm{d}x = \tfrac{1}{|\Omega|}\int_\Omega P_k \mathrm{d}x = \overline{u}_\Omega$$

for $k = 1, \ldots, \widehat{m}$*, then also* P_0 *and* P_{rec} *have the same cell average:*

$$\tfrac{1}{|\Omega|}\int_\Omega P_0\mathrm{d}x = \tfrac{1}{|\Omega|}\int_\Omega P_{\mathsf{rec}}\mathrm{d}x = \overline{u}_\Omega.$$

Remark 3. *The previous definitions may be cast in either one-dimensional or multi-dimensional settings. In the latter case* $x = (x_1, \ldots, x_n) \in \mathbb{R}^n$ *and* $\mathbb{P}^g$ *denotes the space of polynomials in* n *variables with degree at most* g*.*

Typically, in Finite Volume schemes, the optimal polynomial P_{opt} is taken to be the polynomial interpolating all the data in the stencil of the reconstruction in the sense of cell averages. For example in one space dimension, in each cell Ω_j, the original CWENO construction of [LPR99], is a third order accurate CWENO procedure with $\widehat{m} = 2$, $P_{\mathsf{opt}} = P^{(2)}$ the parabola defined on the centered 3-cell stencil $\Omega_{j-1}, \Omega_j, \Omega_{j+1}$, and $P_1 = P_L^{(1)}$, $P_2 = P_R^{(1)}$ being the two linear polynomials interpolating the data in Ω_{j-1}, Ω_j and Ω_j, Ω_{j+1} respectively. The same reconstruction was recently considered in a non-uniform mesh setting in [PS16, CS].

A fifth order version $\mathsf{CWENO}(P^{(4)}, P_L^{(2)}, P_C^{(2)}, P_R^{(2)})$ was proposed in [Cap08], using a centered fourth degree polynomial interpolating the data in $\Omega_{j-2}, \ldots, \Omega_{j+2}$ and the same 3 parabulas employed in the classical WENO5 scheme, namely those interpolating the data in $\Omega_{j-2+r}, \Omega_{j-1+r}, \Omega_{j+r}$ for $r = 0, 1, 2$ respectively.

Along the same lines, in this paper we will introduce a seventh order reconstruction $\mathsf{CWENO}\,7 = \mathsf{CWENO}(P^{(6)}, P_{LL}^{(3)}, P_L^{(3)}, P_R^{(3)}, P_{RR}^{(3)})$, where the optimal

polynomial is the sixth order $P^{(6)} = P_{\mathsf{opt}}$ interpolating the data in $\Omega_{j-3}, \dots, \Omega_{j+3}$ and $P_1 = P^{(3)}_{LL}$, $P_2 = P^{(3)}_{L}$, $P_3 = P^{(3)}_{R}$, $P_4 = P^{(3)}_{RR}$ are the third order polynomials interpolating $\overline{u}_{j-3+r}, \dots, \overline{u}_{j+r}$ for $l = 0, 1, 2, 3$.

Similarly, we will also propose the ninth order reconstruction CWENO 9 with $\widehat{m} = 5$, P_{opt} the eigth order polynomial interpolating the data in $\Omega_{j-4}, \dots, \Omega_{j+4}$ and $P_1, \dots, P_5$ are fourth order polynomials interpolating $\overline{u}_{j-4+r}, \dots, \overline{u}_{j+r}$ for $l = 0, 1, 2, 3, 4$.

A few two-dimensional CWENO reconstructions can be found in the literature, including those of [LPR00] where this technique was proposed and [CRS16] where it is generalized to non cartesian grids.

We note that the coefficients d_k appearing in Definition 2 do not need to satisfy accuracy requirements and they can be thus arbitrarily chosen, provided that they are positive and add up to 1. A possible choice of coefficients is described just below.

We start assigning weights to the low degree polynomials, biasing towards the central ones, because they would yield a smaller interpolation error. A reconstruction of order $G = 2g - 1$ is composed of $\widehat{m} = g + 1$ polynomials of degree g. These are the $\widehat{m}$ polynomials which would compose a WENO reconstruction of order G. Let $j = 1, \dots, \widehat{m}$ be the indices of the low degree polynomials. We start computing temporary weights

$$\tilde{d}_j = \tilde{d}_{\widehat{m}+1-j} = j, \qquad \text{for } 1 \le j \le \frac{\widehat{m}+1}{2}. \tag{11}$$

Then we choose the linear coefficient $d_0 \in (0, 1)$ of the high order polynomial P_0. The final weights are given by

$$d_j = \frac{\tilde{d}_j}{\sum_{i=1}^{\widehat{m}} \tilde{d}_i}(1 - d_0).$$

The value of d_0 must be bounded away from 0 and from 1. In fact, when d_0 is too close to 0 the polynomial P_0 becomes unbounded. On the other hand, when d_0 is close to 1, the reconstruction polynomial P_{rec} will almost coincide with P_{opt}, irrespectively of the oscillation indicators.

In this paper we will mainly consider the two cases $d_0 = \frac{1}{2}$ and $d_0 = \frac{3}{4}$. For instance, when $G = 5$, and $d_0 = \frac{3}{4}$, we have the left and right parabola with weight $d_1 = d_3 = \frac{1}{16}$ and $d_2 = \frac{1}{8}$.

3.1 Implementation of the reconstruction in 1D

The main task for computing a CWENO reconstruction efficiently is to optimize the computation of the coefficients of the interpolating polynomials. In WENO the reconstruction is computed only at one point at a time and thus the Lagrange form of the interpolating polynomials is well suited to the task, see [Shu98]. In contract, here we need the functional representation of the polynomials and therefore it is more convenient to start from the Newton basis and finally get the reprentation of the polynomials in the basis of the monomials.

Let us denote by $\overline{u}_j$ the cell average of $u(x)$ on the generic cell Ω_j of the grid, of size h_j. In order to compute the CWENO reconstruction in the j-th cell, we need the explicit expression of the polynomial of degree k that interpolates the cell averages $\overline{u}_{j-r}, \ldots, \overline{u}_{j-r+k}$. Here r denotes the offset of the stencil with respect to the j-th cell. Note that for a typical CWENO reconstruction one needs $g+1$ polynomials of degree g with $r = 0, \ldots, g$ and a polynomial of degree $2g$ with offset $r = g$. Note also that g out of the $g+1$ polynomials of degree g employed in the reconstruction for cell Ω_j are used also for the reconstruction in the cell Ω_{j+1}, so that one needs to compute only one new polynomial per cell.

It is thus convenient to compute all divided differences of the set of cell averages as a preprocessing stage to the computation of the reconstruction. In particular, denote the *divided differences* of the cell averages by

$$\tilde{\delta}_{j,1} = \overline{u}_j, \qquad \tilde{\delta}_{j,p} = \frac{\tilde{\delta}_{j+1,p-1} - \tilde{\delta}_{j,p-1}}{\sum_{i=j}^{j+p-1} h_i} \text{ for } p > 1. \tag{12}$$

For later convenience, let

$$\delta_{j,p} = \tilde{\delta}_{j,p}\Big|_{\forall i: h_i = 1} \tag{13}$$

These latter are the *undivided differences* which are useful for computations on uniform grids.

Following [Shu98] we note that a polynomials $p(x)$ of degree k interpolating a set of consecutive cell averages can be easily computed by differentiating the polynomial $q(x)$ of degree $k+1$ that interpolate the quantities $S_i = \sum_{l \le i} h_l \overline{u}_l$ in the interpolation nodes $x_i + h_i/2$. It is easy to see that, for the sake of computing $p(x)$, the zero order term in $q(x)$ is not relevant. Thus the only divided differences that are needed are the ones listed in (12).

From now on, let us focus on a reference cell $j = 0$ and assume that its cell center is at $x_0 = 0$. Let $p_r^{(k)}(x)$ be the degree k polynomial with stencil offset r. Applying the Newton interpolation, one finds that its primitive is

$$q_r^{(k+1)}(x) = \sum_{i=1}^{k+1} \tilde{\delta}_{-r,i} \prod_{l=0}^{i-1} (x - x_{-r-1/2+l}) + \text{constant term} \tag{14}$$

and we write it in the basis of the monomials as

$$q_r^{(k+1)}(x) = \sum_{i=1}^{k+1} \tilde{\delta}_{-r,i} \sum_{m=0}^{i} \tilde{\gamma}_{r,i,m}^k x^m + \text{constant term} \tag{15}$$

where $\tilde{\gamma}_{r,i,m}^k$ is the weight of the divided difference of order i and offset $-r$ (i.e. $\tilde{\delta}_{-r,i}$) appearing into the coefficient of the monomial x^m. Note that only the coefficients $\tilde{\gamma}_{r,i,m}^k$ for $m > 0$ appear in the derivative of $q(x)$. By direct comparison of the last two equations one finds for the linear term that

$$\tilde{\gamma}_{r,1,1}^k = 1, \qquad \tilde{\gamma}_{r,i,1}^k = (-1)^{i-1} \sum_{n=0}^{i-1} \prod_{\substack{l=0,\ldots,i-1 \\ l \neq n}} x_{l-r-1/2}, \; i > 1$$

and in general

$$\begin{aligned}
\tilde{\gamma}^k_{r,i,m} &= (-1)^{i-m} \sum_{n_1=0}^{i-1} \sum_{n_2=n_1+1}^{i-1} \cdots \sum_{n_m=n_{m-1}+1}^{i-1} \prod_{\substack{l=0,\ldots,i-1 \\ l\neq n_1,\ldots,n_m}} x_{l-r-1/2}, \quad m < i \\
\tilde{\gamma}^k_{r,m,m} &= 1, \\
\tilde{\gamma}^k_{r,i,m} &= 0, \quad m > i.
\end{aligned} \tag{16}$$

Finally, the sought polynomial $p_r^{(k)}$ is found differentiating $q_r^{(k+1)}$ and it can be written as

$$p_r^{(k)}(x) = \sum_{i=1}^{k+1} \tilde{\delta}_{-r,i} \sum_{m=1}^{i} \tilde{\Gamma}^k_{r,i,m} x^{m-1}, \qquad \tilde{\Gamma}^k_{r,i,m} = m\tilde{\gamma}^k_{r,i,m} \tag{17}$$

Note in particular that the values of $\tilde{\gamma}^k_{r,i,0}$ are not needed in the expression for $p_r^{(k)}(x)$.

Equation (16) can be simplified exploiting the identity

$$x_{l-r-1/2} = -\sum_{i=l-r}^{-1} h_i + \operatorname{sign}(l-r)\frac{h_0}{2} + \sum_{i=1}^{l-r-1} h_i$$

Note also that in the above expression, one of the two summations is always empty, depending on the sign of $l - r$.

Of course considerable simplifications occur on uniform grids, where one can write

$$\begin{aligned}
q_r^{(k+1)}(x) &= \sum_{i=1}^{k+1} \tilde{\delta}_{-r,i} \prod_{l=0}^{i-1} (x - (-r - 1/2 + l)h) + \text{constant term} \\
&= \sum_{i=1}^{k+1} \delta_{-r,i} \prod_{l=0}^{i-1} (\hat{x} - (-r - 1/2 + l)) + \text{constant term}
\end{aligned} \tag{18}$$

where we recall that $\delta_{-r,i}$ are the undivided differences and $\hat{x} = x/h$. The above polynomial can be put in the form (15) with

$$\tilde{\gamma}^k_{r,i,m} = (-h)^{i-m} \sum_{n_1=0}^{i-1} \sum_{n_2=n_1+1}^{i-1} \cdots \sum_{n_m=n_{m-1}+1}^{i-1} \prod_{\substack{l=0,\ldots,i-1 \\ l\neq n_1,\ldots,n_m}} (l - r - 1/2). \tag{19}$$

An alternative form is

$$q_r^{(k+1)}(x) = \sum_{i=1}^{k+1} \delta_{-r,i} \sum_{m=0}^{i} \gamma^k_{r,i,m} x^m + \text{constant term} \tag{20}$$

$$\Gamma_{3,i,m} = \begin{bmatrix} 1 & & & & & & \\ 6 & 2 & & & & & \\ {}^{71}/_{4} & 15 & 3 & & & & \\ 22 & 43 & 24 & 4 & & & \\ -{}^{71}/_{16} & {}^{45}/_{2} & {}^{105}/_{2} & 30 & 5 & & \\ {}^{27}/_{8} & -{}^{341}/_{8} & -45 & 25 & 30 & 6 & \\ -{}^{225}/_{64} & {}^{1813}/_{16} & {}^{777}/_{16} & -{}^{245}/_{2} & -{}^{175}/_{4} & 21 & 7 \end{bmatrix}$$

$$\Gamma_{2,i,m} = \begin{bmatrix} 1 & & & & \\ 4 & 2 & & & \\ {}^{23}/_{4} & 9 & 3 & & \\ -1 & 7 & 12 & 4 & \\ {}^{9}/_{16} & -{}^{25}/_{2} & -{}^{15}/_{2} & 10 & 5 \end{bmatrix}$$

$$\Gamma_{1,i,m} = \begin{bmatrix} 1 & & & \\ 2 & 2 & & \\ -{}^{1}/_{4} & 3 & 3 & \\ 0 & -5 & 0 & 4 \end{bmatrix} \qquad \Gamma_{0,i,m} = \begin{bmatrix} 1 & & & \\ 0 & 2 & & \\ -{}^{1}/_{4} & -3 & 3 & \\ 1 & 7 & -12 & 4 \end{bmatrix}$$

Table 1: Table of the Γ coefficients of (22) used in the computation of CWENO reconstructions up to order 7 on uniform grids.

with

$$\gamma^k_{r,i,m} = (-1)^{i-m} \sum_{n_1=0}^{i-1} \sum_{n_2=n_1+1}^{i-1} \cdots \sum_{n_m=n_{m-1}+1}^{i-1} \prod_{\substack{l=0,\ldots,i-1 \\ l\neq n_1,\ldots,n_m}} (l - r - {}^{1}/_{2}). \tag{21}$$

Finally,

$$p^{(k)}_r(x) = \sum_{i=1}^{k+1} \delta_{-r,i} \sum_{m=0}^{i} \Gamma^k_{r,i,m} x^{m-1}, \qquad \Gamma^k_{r,i,m} = m\gamma^k_{r,i,m} \tag{22}$$

In Table 1 we list the values of the coefficients $\Gamma^k_{r,i,m}$ needed for the CWENO reconstructions up to order 7. The coefficients for the higher order cases can be computed using (22) and (21).

If the final accuracy of the reconstruction is $p = 2g + 1$, we need the stencil $\Omega_{-g}, \ldots, \Omega_g$. Here we must compute the polynomial P_{opt} which has offset g and contains monomials of degree m up to $2g$ and all polynomials of degree $k = g$ with offset $r = 0, \ldots, g$. Note that the elements of $\Gamma^k_{r,i,m}$ are independent of k. Therefore they can all be stored in a matrix $\Gamma_{r,i,m}$ and the coefficients needed for the polynomial of degree k with shift r are in the top-left $(k + 1) \times (k + 1)$ submatrix of the matrix $\Gamma_{r,i,m}$, listed in Table 1.

For example, for CWENO 7, we need all coefficients of $\Gamma_{3,i,m}$ to build P_{opt} and also the top 4×4 submatrices from each $\Gamma_{r,i,m}$ (including $\Gamma_{3,i,m}$) to build the coefficients of the four cubic polynomials which compose the reconstruction.

4 Analysis of the CWENO reconstruction in the smooth case

This topic corresponds to point 2 in the list of Summary 1. In order to perform the analysis of the CWENO reconstruction, let us focus on a fixed computational cell Ω_0 and assume that its cell center is $x_0 = 0$. The CWENO procedure will be applied to the set of exact cell averages $\overline{u}_j$ of a given function $u(x)$. Let us assume that $P_{\mathsf{opt}} \in \mathbb{P}^G$ interpolates the cell averages of Ω_0 and of a suitable number of neighbours, so that its approximation order is $\mathcal{O}(h^{G+1})$, if the function $u(x)$ is sufficiently regular. Furthermore the polynomials $P_r \in \mathbb{P}^g$ are typically chosen to interpolate $g+1 < G+1$ cell averages inside the stencil of P_{opt} and their approximation order is $\mathcal{O}(h^{g+1})$. The reconstruction error at a point $x \in \Omega_0$ is thus given by

$$\begin{aligned} u(x) - P_{\mathsf{rec}}(x) &= u(x) - P_{\mathsf{opt}}(x) + \sum_{r=0}^{\widehat{m}} (d_r - \omega_r) P_r(x) \\ &= \underbrace{(u(x) - P_{\mathsf{opt}}(x))}_{\mathcal{O}(h^{G+1})} + \sum_{r=0}^{\widehat{m}} (d_r - \omega_r) \underbrace{(P_r(x) - u(x))}_{\mathcal{O}(h^{g+1})} \end{aligned} \tag{23}$$

where the last equality is true since $\sum_r d_r = \sum_r \omega_r = 1$. From the above formula it is then clear that the accuracy of the CWENO reconstruction equals the accuracy of its first argument P_{opt} only if $(d_r - \omega_r) = \mathcal{O}(h^{G-g})$ in the case of smooth data, as in standard WENO.

As we will see, CWENO, exactly as WENO, can be influenced by the chosen value chosen for ϵ in (4) and (9). While obviously a value that is too large will promote the onset of spurious oscillations, a value that is too small may induce a degradation of the convergence order close to local extrema. This effect was first noticed in the WENO setting in [HAP05] and a technique consisting in a post-processing of the WENO weights known as WENO-Z was proposed in the same paper and later extended to higher order in [FHW14]. Another approach involving additional smoothness indicators, known as WENO-Z has also been studied (see [DB13] and references therein). In [ABBM11] the authors devise a way to relate the value of ϵ to the mesh size in order to guarantee the correct convergence order and this technique has been extended to the CWENO setting in [Kol14] for uniform meshes and exploited also on non-uniform meshes in one and two space dimensions, [CS] and [CRS16], respectively.

Qui ci sono due WENO-Z che fanno cose diverse. Da correggere

For this reason we are mainly interested in the choice

$$\epsilon = \hat{\epsilon} h^p, \text{ for } p = 1, 2 \tag{24}$$

where h is the mesh size.

We state here a general result on the accuracy of the polynomial P_0 computed in step 1 of the CWENO reconstruction.

Remark 4. *P_0 is of degree G, but its accuracy is:*

$$\begin{aligned} P_0(x) - u(x) &= \frac{1}{d_0}\left[P_{\mathsf{opt}}(x) - \sum_{r\geq 1} d_r P_r(x) - d_0 u(x)\right] \\ &= \frac{1}{d_0}\left[P_{\mathsf{opt}}(x) - \sum_{r\geq 1} d_r P_r(x) - \left(1 - \sum_{r\geq 1} d_r\right) u(x)\right] \\ &= \frac{1}{d_0}\Big(P_{\mathsf{opt}}(x) - u(x)\Big) + \frac{\sum_{r\geq 1} d_r}{d_0}\Big(u(x) - P_r(x)\Big). \end{aligned}$$

Thus the accuracy of P_0 will coincide with the smallest accuracy of the P_r's.

In order to prove that the accuracy of CWENO is $\mathcal{O}(h^{G+1})$ on smooth data, one has to show that $\omega_r - d_r$ is at least $\mathcal{O}(h^{G-g})$. This study can be performed extending to our case the technique introduced by [ABBM11] in the case of WENO and which allows to rewrite $\omega_r - d_r$ in terms of differences among the indicators of the candidate polynomials.

The CWENO procedure starts by computing

$$\begin{aligned} \alpha_0 &= \frac{d_0}{(\epsilon + I[P_0])^t} \\ \alpha_r &= \frac{d_r}{(\epsilon + I[P_r])^t} = \frac{d_r}{(\epsilon + I[P_0])^t}\left[1 + \frac{I[P_0] - I[P_r]}{\epsilon + I[P_r]} \sum_{s=0}^{t-1}\left(\frac{\epsilon + I[P_0]}{\epsilon + I[P_r]}\right)^s\right], r = 1, \ldots, \widehat{m} \end{aligned} \tag{25}$$

In order to proceed, we need the Taylor expansions of the differences between the indicators $I[P_r]$ for $r = 0, \ldots, \widehat{m}$ and we focus on the classical Jiang-Shu indicators of (6). First note that the Jiang-Shu indicator in terms of the coefficients of a generic polynomial, centered in 0, is given by

$$I\left[\sum_{i=0}^{g} a_i x^i\right] = \sum_{l=1}^{g}\sum_{j=l}^{g-1}\sum_{\substack{i=j,\\ i+j \text{ even}}}^{g} \frac{j!i!}{(j-l)!(i-l)!}\frac{2^{2l+1-j-i-\delta_{i,j}}}{j+i-2l+1} a_j a_i h^{j+i} \tag{26}$$

where $\delta_{i,j}$ denotes the Kronecker delta.

If the polynomial $\sum_{i=0}^{g} a_i x^i$ of degree g is interpolating the cell averages of a smooth enough function $u(x)$, then its coefficients satisfy

$$a_i = \frac{1}{i!}u^{(i)}(0) + \mathcal{O}(h^{g-i+1}), \qquad i = 0, 1, \cdots, g. \tag{27}$$

If the polynomial is centred in 0, as in the formula above, then the property above requires the derivative to be evaluated in 0, not in x_0, otherwise one should write the polynomials as $\sum a_i(x - x_0)^i$, but I don't know where the x_0 would eventually go in the formulas. This is why I chose to compute all derivatives in 0.

Note that (27) holds true also for the polynomial $P_0 \in \mathbb{P}^G$, but only for $i = 0, \dots, g$. In fact, letting $P_{\mathsf{opt}} = \sum_0^G b_i x^i$ and $P_r = \sum_0^g a_{r,i} x^i$ and using the definition of P_0, one finds

$$P_0(x) = \sum_{i=0}^{G} a_{0,i} x^i = \sum_{i=0}^{G} \left(\frac{b_i}{d_0} - \sum_{r=1}^{\widehat{m}} a_{r,i} \frac{d_r}{d_0} \right) x^i.$$

Next, using (27) for P_{opt} and P_r for $r = 1, \dots, \widehat{m}$ one gets

$$a_{0,i} = \frac{1}{d_0 i!} \left(\left(1 - \sum_{r=1}^{\widehat{m}} d_r \right) u^{(i)}(0) + \mathcal{O}(h^{g-i+1}) \right)$$

and finally

$$a_{0,i} = \frac{1}{i!} u^{(i)}(0) + \mathcal{O}(h^{g-i+1}), \qquad i = 0, \dots, g. \tag{28}$$

It follows that for $r = 0, \dots, \widehat{m}$,

$$I[P_r] = \sum_{l=1}^{g} \sum_{j=l}^{g-1} \sum_{\substack{i=j, \\ i+j<g+2, \\ i+j \text{ even}}}^{g} \frac{j!}{(j-l)!(i-l)!} \frac{2^{2l+1-j-i-\delta_{i,j}}}{j+i-2l+1} u^{(j)}(0) u^{(i)}(0) h^{j+i} + \mathcal{O}(h^{g+2}). \tag{29}$$

We now turn to the terms appearing in (25). Recalling (24) and (29), we have

$$\sum_{s=0}^{t-1} \left(\frac{\epsilon + I[P_0]}{\epsilon + I[P_r]} \right)^s = \sum_{s=0}^{t-1} \left(\frac{\hat{\epsilon} h^p + I[P_0]}{\hat{\epsilon} h^p + I[P_r]} \right)^s = t + \mathcal{O}(h^{g+2-p}). \tag{30}$$

Perche' nella 29 c'e' un j! scritto in blu?

Qui, e nel seguito, mi aspetterei di veder comparire almeno $u'(0)$, o almeno a_1. Mi sembra che se a_1 sia uguale a zero dovrebbe cambiare qualcosa, ma è puramente a naso, perché ammetto che i vostri conti non li ho rifatti.

For the terms

$$\frac{I[P_0] - I[P_r]}{\epsilon + I[P_r]} \tag{31}$$

we observe that (29) holds true for all polynomials involved in the reconstruction. Thus for the numerator we have that

$$I[P_0] - I[P_r] = \mathcal{O}(h^{g+2}).$$

Instead for the denominator of (31), we observe that (26) implies that $I[P_r] = a_1^2 h^2 + \mathcal{O}(h^4)$ and, recalling the choice of ϵ in (24), we find

$$\hat{\epsilon} h^p + I[P_r] = A h^p \left(1 + \sum_{l=1}^{g} \sum_{\substack{j=l \\ j \neq p-1}}^{g-1} \sum_{\substack{i=j, \\ i+j \text{ even}}}^{g} \frac{j! i!}{(j-l)!(i-l)!} \frac{2^{2l+1-j-i-\delta_{i,j}}}{j+i-2l+1} \frac{a_j a_i}{A} h^{j+i-p} \right)$$

where $A = \hat{\epsilon}$ if $p = 0, 1$ and $A = \hat{\epsilon} + a_1^2$ if $p = 2$. Now

$$\frac{1}{\hat{\epsilon}h^p + I[P_r]} = \frac{1}{Ah^p}\left(1 + \mathcal{O}(h^p)\right)$$

so that

$$\frac{I[P_0] - I[P_r]}{\epsilon + I[P_r]} = \frac{\mathcal{O}(h^{g+2})}{Ah^p}\left(1 + \mathcal{O}(h^p)\right) = \mathcal{O}(h^{g+2-p})$$

Recalling (30) and (25), we have

$$\begin{aligned}\sum_0^{\widehat{m}} \alpha_r &= \frac{1}{(\epsilon + I[P_0])^t}\left[1 + \sum_0^{\widehat{m}} d_r \frac{I[P_0] - I[P_r]}{\epsilon + I[P_r]} \sum_{s=0}^{t-1} \left(\frac{\epsilon + I[P_0]}{\epsilon + I[P_r]}\right)^s\right] \\ &= \frac{1}{(\epsilon + I[P_0])^t}\left[1 + \mathcal{O}(h^{g+2-p})\left(t + \mathcal{O}(h^{g+2-p})\right)\right] \\ &= \frac{1}{(\epsilon + I[P_0])^t}\left[1 + \mathcal{O}(h^{g+2-p})\right]\end{aligned}$$

and thus

$$\frac{1}{\sum_{i=0}^{\widehat{m}} \alpha_i} = (\epsilon + I[P_0])^t\left[1 + \mathcal{O}(h^{g+2-p})\right].$$

Finally, using (25) and the previous relation we have

$$\omega_r = \frac{\alpha_r}{\sum_{s=0}^{\widehat{m}} \alpha_s} = d_r\left[1 + \mathcal{O}(h^{g+2-p})\right]. \tag{32}$$

Questo non è un todo: è una confessione: mi fido di voi e non ho rifatto i conti

We thus have the following

Proposition 1. *The* CWENO *reconstruction with* P_{opt} *of degree* G *and* $P_1, \ldots, P_{\widehat{m}}$ *of degree* g *is* $2G$ *order accurate on smooth solutions, provided that* $G \leq 2g$ *and* $\epsilon = \hat{\epsilon}h^p$ *with* $p = 0, 1, 2$.

Proof. The above discussion leading to equation (32) shows that $\omega_k - d_k = \mathcal{O}(h^{g+2-p})$ and thus the accuracy is maximal provided that $g+2-p \geq G-g$. □

Dice Matteo: Verificare $p = 0$. Se non funziona, toglierlo e mettere invece qui un Remark in cui si dice che con $p = 0$ tutto funziona almeno quando $\hat{\epsilon} \ll h^2$. Forse è più facile che introdurre il caso $p = 0$ perché a questo punto quale dei due sia il termine dominante nei raccoglimenti dipende dalla grandezza relativa di $\hat{\epsilon}$ e degli $I[P]$.

Anche perchè, aggiungo ancora io (G), da quanto si scrive sopra sembrerebbe che $p = 0$ sia proprio la scelta ottimale. Questa storia di $p = 0$ va un po' ripensata, anche se le osservazioni sotto mi sembrano motivi sufficienti per non prendere $p = 0$.

We point out that, starting from (27), all expressions hold in the limit $h \to 0$. Obviously, for finite values of h, the behaviour of the reconstruction is determined by the relative size of $\hat{\epsilon}h^p$ and the indicators. Especially in the case $p = 0$, when $\hat{\epsilon}$ is too small with respect to h, one typically observes a degradation in

Dice Matteo: Verificare che valga anche per $p = 0$ ed eventualmente aggiustare.

Aggiungo io (G): ma se queste stime valgono anche per $p = 0$, perchè la gente si dovrebbe dannare con gli ϵ? Eppure si sa che con $\epsilon = ch^0$ l'accuratezza può saltare. O forse salta solo per WENO e non per noi?

the convergence rate. On the other hand, if $\hat{\epsilon}$ is too large, one might observe spurious oscillations, since $\hat{\epsilon}$ would override the indicators.

Another case where the size of ϵ can change the behaviour of the reconstruction is close to a local extremum. It typically happens that the local extremum does not lie in the stencil of all P_r's. Suppose that an extremum is located only in the stencil of $P_{\hat{r}}$ for some $\hat{r} \in \{1, \dots, \widehat{m}\}$. In this case, we would have $I[P_{\hat{r}}] = \mathcal{O}(h^4)$ but $I[P_r] \asymp h^2$ for $r \neq \hat{r}$. Unless $\epsilon + h^4 \ll \epsilon + h^2$, the computation of the non-linear weights will give $\omega_{\hat{r}} \approx 1$ and $\omega_r \approx 0$ for $r \neq \hat{r}$ and the reconstruction would be of order g instead of being of order G. For this reason we suggest to employ $\epsilon \approx h^2$ or even $\epsilon \approx h$, as in [CS, CRS16].

5 Analysis in the discontinous case

This section contains a discussion of the behaviour of CWENO in the case of discontinuous data. While the discussion of the previous section on the smooth case extends to reconstructions of arbitrary order of accuracy, partial contributions of previous authors, the discontinous case, to the best of our knowledge, has never been analyzed in detail. In this section we will consider CWENO as an interpolation algorithm, of a known function $u(x)$. Thus we will suppose that it is possible to choose the mesh size to ensure that at most one discontinuity is present in the stencil of P_{opt}.

If a discontinuity is present in the stencil of P_{opt}, then the reconstruction is expected to degrade to a combination of the P_k's whose stencil lie in smooth regions. In this respect, the reconstruction behaves as WENO. In the WENO setting, this fact is almost trivial: only the P_k's contribute to the reconstruction and they are all interpolating polynomials, thus the behaviour of their indicators matches exactly the presence or absence of a discontinuity in the corresponding stencil.

In the CWENO setting, the same final result can be proven only if an additional property is verified by the indicators. In fact, in CWENO, also the high order polynomial P_0 contributes non trivially to P_{rec} and thus the behaviour of its indicator should be taken into account as well. However, P_0 is not an interpolating polynomial and thus, for the correct behaviour of the reconstruction in the discontinuous case, it is important that the following holds.

Definition 3 (Property R). *We say that a reconstruction* $\mathsf{CWENO}(P_{\mathsf{opt}}, P_1, \dots, P_{\widehat{m}})$ *satisfies Property R if* $I[P_{\mathsf{opt}}] \asymp 1$ *when* $h \to 0$ *implies that also* $I[P_0] \asymp 1$.

We will prove that Property R holds in each individual case. Here we show a general result of the impact of Property R on the behaviour of CWENO on discontinuous data.

Theorem 1. *Assume that Property R holds true for a* CWENO *procedure. If the reconstruction is applied to discontinuous data, but at least one of* $I[P_1], \dots, I[P_{\widehat{m}}]$ *is of size* $\mathcal{O}(h^2)$*, then* $\omega_k \sim 0$ *for every* $k \in \{0, \dots, \widehat{m}\}$ *such that* $I[P_k] \asymp 1$.

Proof. Since the data are discontinuous, then $I[P_{\mathsf{opt}}] \asymp 1$ and, thanks to Property R, also $I[P_0] \asymp 1$. Let K be the set $\{k : I[P_k] \asymp 1\}$. Then the hypothesis guarantees that there exists at least one $l \notin K$ for which $I[P_l] = \mathcal{O}(h^2)$. Therefore α_l is at least of magnitude h^{-2} and thus from (9) we find that $\omega_l \asymp 1$ and $\omega_k = \mathcal{O}(h^2)$ for every $k \in K$. □

As a corollary, provided that at least one of $P_1, \dots, P_{\widehat{m}}$ insists on a smooth stencil, the reconstruction degrades to a combination of the P_k's with smooth stencil and thus will be Essentially Not Oscillatory. With reference to Summary 1, Property R corresponds to point 1 and Theorem 1 to point 3.

Notice that Property R is not trivial, despite the fact that P_0 is a convex combination of the interpolating polynomials P_{opt} and of all the P_k's. In fact, at least for the Jiang-Shu indicators, the square inside the integrals in equation (6) mixes in a nonlinear way the contributions of all the polynomials involved. For example, even with $\widehat{m} = 1$, we have $P_0 = \alpha P_{\mathsf{opt}} + (1-\alpha)P_1$ (for $\alpha = 1/d_0$) and

$$I[P_0] = \alpha^2 I[P_{\mathsf{opt}}] + (1-\alpha)^2 I_{P_1} + \alpha(1-\alpha) \sum_{l \geq 1} \operatorname{diam}(\Omega)^{2l-1} \int_\Omega P_{\mathsf{opt}}^{(l)}(x) P_1^{(l)}(x) \mathrm{d}x. \tag{33}$$

In the formula above, $I[P_{\mathsf{opt}}]$ and $I[P_1]$ are always non-negative, but there is no way to control the sign of the cross terms.

When proving that Property R holds, we have to prove that, when a discontinuity occours in the stencil, the ratio of the indicators of P_0 and P_{opt} is finite and stays away from zero. Typically it is easy to compute explicitly and study the ratio of the indicators if the data are the cell averages of a Heaviside function with the jump located inside the reconstruction stencil. We thus prove now a perturbation result that will allow us to extend easily our proofs from the Heaviside data to the general case.

Lemma 1. *Consider $u(x) = H(x) + v(x)$ where $H(x)$ is the Heaviside function and $v(x)$ a Lipschitz continuous function. Let P_1 and P_2 denote polynomials depending smoothly on the cell averages of $u(x)$ such that both $I[P_1] \asymp 1$ and $I[P_2] \asymp 1$. Then*

$$\frac{I[P_1]}{I[P_2]} = \left.\frac{I[P_1]}{I[P_2]}\right|_{v \equiv 0} + \mathcal{O}(h)$$

when the cell size $h \to 0$.

Proof. The thesis follows easily from Remark 1, which implies that $I[P] = I[P]|_{v\equiv 0} + \mathcal{O}(h)$. □

We now turn to the verification of Property R on CWENO reconstructions of order $3, 5$ and 7 with weights chosen simmetrycally. Note that in particular this is the case if the weights are chosen according to equation (11). The CWENO 9 scheme can be handled similarly, but the computations become quite cumbersome.

We start from the case in which the discontinuity in the data does not occour in the central cell.

5.1 CWENO 3

We start from the third order CWENO reconstruction of [LPR99]. We recall that in this case the stencil consists of the three cells $\Omega_{j+l}, l = -1, 0, 1$, $P^{(2)} = P_{\mathsf{opt}} \in \mathbb{P}^2$ is the parabola interpolating in the sense of cell averages a given function $u(x)$ on the whole stencil, while $P_L^{(1)}$ and $P_R^{(1)}$ are the two left and right linear functions interpolating the cell averages $\overline{u}_{j-1}, \overline{u}_j$ and $\overline{u}_j, \overline{u}_{j+1}$, respectively.

Proposition 2. *Consider the operator* $\mathsf{CWENO}(P^{(2)}, P_L^{(1)}, P_R^{(1)})$*, with* $d_L = d_R$*. Suppose that a discontinuity is present in the stencil of the reconstruction, but does not occour in the central cell, then*

$$\frac{I[P_0]}{I[P_{\mathsf{opt}}]} = \frac{I[P_0]}{I[P^{(2)}]} > \frac{13}{16} \quad (\textit{and thus } I[P_0] \asymp I[P_{\mathsf{opt}}]).$$

Proof. Thanks to Lemma 1, we may restrict the analysis to the application of CWENO to the cell averages of a Heaviside function. Using the hypothesis on the location of the discontinuity, without loss of generality, we consider

$$\overline{u}_{j-1} = 1 \qquad \overline{u}_j = 0 \qquad \overline{u}_{j+1} = 0.$$

In this case, by direct computation one finds that

$$\frac{I[P_0]}{I[P^{(2)}]} = \frac{3d_0^2 - 6d_0 + 16}{16d_0^2}. \tag{34}$$

Since the derivative of (34) vanishes at $d_0 = 16/3$ and $d_0 \in [0, 1]$, this expression attains its minimum on the boundary and precisely at $d_0 = 1$, where it attains the value $13/16$. Moreover, this ratio is clearly continuous provided $d_0 \geq \delta > 0$. Thus we have that for every choice of $0 < \delta \leq d_0 \leq 1$, $I[P_0] \asymp 1$ whenever $I[P^{(2)}] \asymp 1$.

Mi è venuto un dubbio: dire $I[P_0] \asymp 1$ whenever $I[P^{(2)}] \asymp 1$ mi sembra voglia dire sia che $\frac{I[P_0]}{I[P^{(2)}]}$ debba essere bounded away from zero, che è quello che con santa pazienza avete dimostrato, sia che quel rapporto deve essere bounded, che invece manca. In realtà è molto semplice: basta dire che il rapporto è continuo e limitato se d_0 è bounded away from zero. Ho aggiunto questa precisazione a tutte le properties che dimostrano la proprietà R. Per far questo, bisogna tagliare via una fettina di spessore $\delta > 0$, cioè $d_0 \geq \delta > 0$, che mi sembra davvero innocuo. Se vi sembra che non serva, togliete queste aggiunte.

□

5.2 CWENO 5

We now turn to CWENO 5. We recall that in this case the stencil consists of the five cells $\Omega_{j+l}, l = -2, \ldots, 2$, $P^{(4)} = P_{\mathsf{opt}} \in \mathbb{P}^4$ is the quartic interpolating in the sense of cell averages a given function $u(x)$ on the whole stencil, while $P_L^{(2)}$, $P_C^{(2)}$ and $P_R^{(2)}$ are the three left, central and right parabolas interpolating the cell averages $\overline{u}_{j-2}, \overline{u}_{j-1}, \overline{u}_j$; $\overline{u}_{j-1}, \overline{u}_j, \overline{u}_{j+1}$ and $\overline{u}_j, \overline{u}_{j+1}, \overline{u}_{j+2}$, respectively.

In the paper [Cap08], the linear coefficients are fixed to $d_0 = 1/2, d_L = 1/8, d_C = 1/4, d_R = 1/8$, but here we assume only that they are symmetric, namely that $d_L = d_R = (1 - d_0 - d_C)/2$.

Proposition 3. *Consider the operator* $\mathsf{CWENO}(P^{(4)}, P_L^{(2)}, P_C^{(2)}, P_R^{(2)})$ *, with* $d_L = d_R$*. Suppose that a discontinuity is present in the stencil of the reconstruction, but does not occour in the central cell, then*

$$\frac{I[P_0]}{I[P_{\mathsf{opt}}]} = \frac{I[P_0]}{I[P^{(4)}]} > 0.6 \quad (\textit{and thus } I[P_0] \asymp I[P_{\mathsf{opt}}]).$$

Proof. Thanks to Lemma 1, we may restrict the analysis to the case of the cell averages of a Heaviside function. Since we only know that the discontinuity is not in the central cell, without loss of generality, we take

$$\overline{u}_{j-2} = 1 \qquad \overline{u}_{j-1} = D \in [0,1] \qquad \overline{u}_j = 0 \qquad \overline{u}_{j+1} = 0 \qquad \overline{u}_{j+2} = 0.$$

Observe that as D grows from 0 to 1 the discontinuity moves from the interface between Ω_{j-2} and Ω_{j-1} to the interface between Ω_{j-1} and Ω_j. With the help of Matlab's symbolic toolbox, we computed the desired ratio $R(d_0, d_C; D) := I[P_0]/I[P_{\mathsf{opt}}]$ which is given by

$$\begin{aligned} R(d_0, d_C; D) = (&10500D^2d_0^2 + 26880D^2d_0d_C - 28896D^2d_0 + 23100D^2d_C^2 - 52752D^2d_C \\ &+ 123359D^2 - 7980Dd_0^2 - 20160Dd_0d_C + 21672Dd_0 - 12180Dd_C^2 \\ &+ 27216Dd_C - 64693D + 1680d_0^2 + 3360d_0d_C - 3612d_0 \\ &+ 1680d_C^2 - 3612d_C + 8840)/(d_0^2(104963D^2 - 51001D + 6908)). \end{aligned} \tag{35}$$

We need to show that the above ratio is finite and bounded away from 0. To this end we study its extrema. Solving $\frac{\partial R}{\partial d_0} = 0$ with respect to d_0, one finds

$$\begin{aligned} d_0 = z(d_C; D) := (&-23100D^2d_C^2 + 52752D^2d_C - 123359D^2 + 12180Dd_C^2 - 27216Dd_C \\ &+ 64693D - 1680d_C^2 + 3612d_C - 8840)/(42(40d_C - 43)(8D^2 - 6D + 1)). \end{aligned}$$

We show that $z(d_C, D) \notin [0,1]$, for any $(d_C, D) \in [0,1]^2$ and thus the minima and maxima of R occour only along the boundary of $[0,1]^2$. First, $z(d_C, D) \neq 0$. In fact, solving $z(d_C, D) = 0$ with respect to D, we would obtain real solutions only if $\Delta_1 \geq 0$, where

$$\Delta_1 = -21(60d_C^2 - 80d_C + 287)(5460d_C^2 - 12768d_C + 29333),$$

which is negative for all $d_C \in [0,1]$. Next, $z(d_C, D) \neq 1$ since, solving $z(d_C, D) = 1$ with respect to D, we would obtain real solutions only if $\Delta_2 \geq 0$, where

$$\Delta_2 = -21(327600d_C^4 - 1202880d_C^3 - 3810840d_C^2 + 4855216d_C - 7797307). \tag{36}$$

A plot of Δ_2 with respect to d_C is shown in Figure 1a, which shows that Δ_2 is negative for all $d_C \in [0,1]$. Finally, observe that $z(d_C, D)$ has an essential

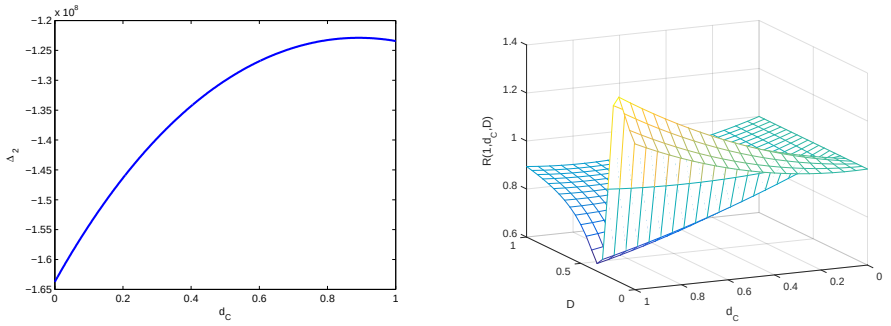

(a) (b)

Figure 1: Supporting graphs for the proof of Proposition 3. Left: the function $\Delta_2(d_C)$ is always negative in $[0,1]$, see (36). Right: plot of $R(1,d_C;D)$ of (34) on $[0,1]^2$, showing that $R > 0.6$

discontinuity in $D = 1/4$ and in $D = 1/2$, but it is otherwise continuous. It thus suffices to show that $z(d_C, D)$ is outside $[0,1]$ in each of the strips $[0,1]\times[0,1/4]$, $[0,1]\times[1/4,1/2]$ and $[0,1]\times[1/2,1]$. Since we have already shown that z cannot cross 0 and 1, we just evaluate z in a point in each strip. We find

$$z(1/2,0) > 1, \quad z(1/2,3/8) < 0, \quad z(1/2,1) > 1,$$

and therefore we can conclude that $z(d_C, D) \notin [0,1]$, for all $(d_C, D) \in [0,1]^2$.

The above argument shows that R has no extrema for $d_0 \in [0,1]$, and therefore it is monotone with respect to d_0 in the domain of interest. Furthermore, it is easy to verify that the denominator in (35) never vanishes and thus R is continuous, except at $d_0 = 0$, where $R \to +\infty$. Therefore R must be decreasing with respect to d_0 and as a consequence, it attains its minimum for $d_0 = 1$. To evaluate this minimum, in Figure 1b, we plot the restriction of R to the domain $d_0 = 1$ and $(d_C, D) \in [0,1]^2$ from which it is clear that the minimum is always larger than 0.6, thus concluding the proof.

If the jump discontinuity is located in the cell Ω_{j-2}, one computes

$$R(d_0, d_C, D = 0) = (420d_0^2 + 840d_0d_C - 903d_0 + 420d_C^2 - 903d_C + 2210)/(1727d_0^2).$$

Note that $R(1, d_C, D)$ can also be studied analytically and, by lengthy computations, one finds the exact location of the minimum and its corresponding value which is $\min(R(1, d_C, D)) \approx 0.632$.

Moreover, R is clearly continuous provided $d_0 \geq \delta > 0$. Thus we have that for every choice of $0 < \delta \leq d_0 \leq 1$, $I[P_0] \asymp 1$ whenever $I[P^{(4)}] \asymp 1$. □

5.3 CWENO 7

We now consider the CWENO 7 reconstruction. We recall that in this case the stencil consists of the seven cells $\Omega_{j+l}, l = -3,\dots,3$, $P^{(6)} = P_{\text{opt}} \in \mathbb{P}^6$

is the sixth degree polynomial interpolating in the sense of cell averages a given function $u(x)$ on the whole stencil. The reconstruction can be written as $\mathsf{CWENO}(P^{(6)}, P^{(3)}_{LL}, P^{(3)}_{L}, P^{(3)}_{R}, P^{(3)}_{RR})$, where the $P^{(3)}$ are cubic polynomials interpolating in the sense of cell averages the function $u(x)$ on the stencil $\Omega_{j-r}, \ldots, \Omega_{j-r+3}$, with $r = 3$ for $P^{(3)}_{LL}$, $r = 2$ for $P^{(3)}_{L}$, $r = 1$ for $P^{(3)}_{R}$, and $r = 0$ for $P^{(3)}_{RR}$.

To carry out the analysis of the discontinuous case for this reconstruction, we need to verify that Property R holds also for the CWENO 7 procedure. To this end, we first state the following Lemma in order to show a general property satisfied by the ratio $I[P_0]/I[P_{\mathsf{opt}}]$ and then we prove Proposition 4 below for a particular position of the jump discontinuity in the reconstruction stencil.

Lemma 2. *Let the linear coefficients $\{d_k\}_{k=LL,L,R,RR}$ of the* CWENO 7 *procedure be linear functions of the coefficient d_0. Then*

$$\frac{\partial}{\partial d_0}\frac{I[P_0]}{I[P_{\mathsf{opt}}]} = \frac{\mathcal{L}(d_0)}{d_0^3}$$

where $\mathcal{L}(d_0)$ is a linear function of d_0.

Proof. Since the coefficients $\{d_k\}_{k=LL,L,R,RR}$ are linear functions of d_0, say $d_k = \mathcal{L}_k(d_0)$, we can write (see Definition 2)

$$P_0(x) = \frac{P_{\mathsf{opt}}(x) - \sum_k \mathcal{L}_k(d_0) P_k(x)}{d_0}.$$

Recalling that P_{opt} does not depend on the d_k's and that the polynomials enter in the Jiang-Shu indicator (6) at most quadratically, we can write

$$\frac{I[P_0]}{I[P_{\mathsf{opt}}]} = \frac{Q(d_0)}{d_0^2}$$

where $Q(d_0)$ is a quadratic function of d_0. The thesis now follows easily. □

Remark 5. *The above Lemma requires that the linear coefficients d_k be linear functions of d_0. Since* CWENO 7 *has many free coefficients, requiring a linear relation among them does not seem to be overly restrictive. Note also that the linear dependence of the other coefficients on d_0 already occurs in* CWENO 3 *and* CWENO 5 *for reasons of symmetry. In the case of* CWENO 7 *the following reasonable choices of the linear coefficients satisfy the hypothesis of the Lemma:*

$$d_{LL} = d_L = d_R = d_{RR}, \qquad 2d_{LL} = d_L = d_R = 2d_{RR}.$$

The second of these is the setup considered in the numerical tests. In this case, the central two cubics are weighted more than the two external ones, because they will provide a smaller interpolation error.

Proposition 4. *Consider* $\mathsf{CWENO}(P^{(6)}, P^{(3)}_{LL}, P^{(3)}_{L}, P^{(3)}_{R}, P^{(3)}_{RR})$*, with* d_{LL}, d_L, d_R *and* d_{RR} *depending linearly on* d_0*. Assume further that the coefficients are chosen respecting the following symmetries:* $d_L = d_R$ *and* $d_{LL} = d_{RR}$*. Suppose that a discontinuity is present in the stencil of the reconstruction, but does not occour in the central cell, then*

$$I[P_0] \asymp I[P^{(6)}] = I[P_{\mathsf{opt}}].$$

Proof. Thanks to Lemma 1, we may restrict the analysis to the case of the cell averages of a Heaviside function. Observe that the statement has to be proved for three different positions of the jump discontinuity, which can be located in the cell Ω_k, for $k = j-3, j-2, j-1$ (and obviously in symmetric positions to the right of Ω_j). Without loss of generality, we need to consider two different cases:

$$\overline{u}_{j-3} = 1 \qquad \overline{u}_{j-2} = D \in [0,1] \qquad \overline{u}_{j-1} = \overline{u}_j = \overline{u}_{j+1} = \overline{u}_{j+2} = \overline{u}_{j+3} = 0.$$

and

$$\overline{u}_{j-3} = \overline{u}_{j-2} = 1 \qquad \overline{u}_{j-1} = D \in [0,1] \qquad \overline{u}_j = \overline{u}_{j+1} = \overline{u}_{j+2} = \overline{u}_{j+3} = 0.$$

In the first case, as D moves from 0 to 1, the discontinuity moves from the interface between Ω_{j-3} and Ω_{j-2}, to the interface between Ω_{j-2} and Ω_{j-1}, while in the second case, as D moves from 0 to 1, the jump moves from the interface between Ω_{j-2} and Ω_{j-1}, to the interface between Ω_{j-1} and Ω_j.

Case 1 Here, we start showing the explicit computations for the first case, namely when the jump discontinuity is located in the cell Ω_{j-2}.

Let $d := d_L = d_R$ and $d_{LL} = d_{RR} = (1 - d_0 - 2d)/2$. Computing the indicators of $P_0(x)$ and $P_{\mathsf{opt}}(x)$, one finds that

$$\begin{aligned} R(d_0, d, D) := \frac{I[P_0]}{I[P_{\mathsf{opt}}]} =& (439271910D^2d_0^2 + 1936962720D^2d_0d - 1100058300D^2d_0 \\ &+ 2183448960D^2d^2 - 2513221920D^2d + 3588778953D^2 \\ &- 242120340Dd_0^2 - 1030102920Dd_0d + 582205635Dd_0 \\ &- 1091724480Dd^2 + 1242687600Dd - 1310085264D \\ &+ 34116390d_0^2 + 136465560d_0d - 76797765d_0 \\ &+ 136465560d^2 - 153595530d + 126751871)/ \\ &(d_0^2(2927992563D^2 - 969999969D + 84070496)). \end{aligned}$$

We need to show that the above ratio never vanishes, for $d_0 \in (0,1]$. To this end we study its extrema. Thanks to the previous lemma, $\frac{\partial R}{\partial d_0} = 0$ leads to a linear equation in d_0, whose solution is

$$\begin{aligned} d_0 = z(d, D) :=& (4366897920D^2d^2 - 5026443840D^2d + 7177557906D^2 - 2183448960Dd^2 \\ &+ 2485375200Dd - 2620170528D + 272931120d^2 - 307191060d \\ &+ 253503742)/(495(4D-1)(555585D + 275688d - 978264Dd - 155147)). \end{aligned}$$

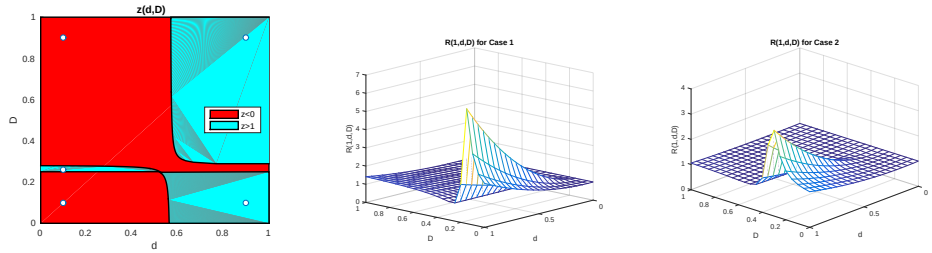

(a) (b) (c)

Figure 2: Supporting graphs for the proof of Proposition 4. Left: domains where $z(d, D)$ is negative and above 1 for Case 1. Middle: plot $R(1, d, D)$ for Case 1 on $[0, 1]^2$ showing that $R > 0.9$. Right: plot $R(1, d, D)$ for Case 2 on $[0, 1]^2$ showing that $R > 0.9$.

In order to show that $z(d, D) \notin [0, 1]$, for any $(d, D) \in [0, 1]^2$, we prove that there cannot be an extremum inside the interval $[0, 1]$. We follow the same line of argument already used in the proof of Proposition 3. First, $z(d, D) \neq 0$ since, solving $z(d, D) = 0$ with respect to D, we obtain a second degree equation with discriminant

$$\Delta_1 = -11(518448774382920d^2 - 563258885649790d + 260642395562461),$$

which is negative for all $d \in \mathbb{R}$. Next, $z(d, D) \neq 1$ since, solving $z(d, D) = 1$ with respect to D, we obtain a second degree equation with discriminant

$$\Delta_2 = -11(8222158841526720d^2 - 4065334566415120d + 1438597144251301),$$

which is again negative for all $d \in \mathbb{R}$. Finally, observe that $z(d, D)$ has essential discontinuities on $D = 1/4$ and along the curve $D = (275688d-155147)/(978264d-555585)$. The above curves divide the square $[0, 1]^2$ in five regions in which z is continuous. Evaluating z at a point in each of these regions (see Fig 2a) we find

$$z(0.1, 0.1) > 1, \quad z(0.9, 0.1) < 0, \quad z(0.1, 0.9) > 1, \quad z(0.9, 0.9) < 0, \quad z(0.1, 0.26) < 0$$

and thus z never takes values in $[0, 1]$ for all $(d, D) \in [0, 1]^2$.

The above argument shows that R, for each $(d, D) \in [0, 1]^2$ fixed, is monotone with respect to d_0 in the domain of interest. Furthermore, the denominator in the definition of R does never vanish and thus R is continuous, except at $d_0 = 0$, where $R \to +\infty$. Thus R must be decreasing with respect to d_0 and therefore its minimum must occour in $d_0 = 1$. Finally, the restriction of R to the domain $d_0 = 1$ and $(d, D) \in [0, 1]^2$ is shown in Figure 2b and it is clear that it is always bounded away from 0, thus concluding the proof of case 1.

The function $R(1, d, D)$ can also be studied analytically and, with lengthy computations, one can find the exact location of the minimum and that its value is approximately 0.978.

Case 2 Similar considerations hold for the case of the jump discontinuity located in the cell Ω_{j-1}. In fact, one can prove again that the extremum is in the restriction of R to the domain $d_0 = 1$ and it is always bounded away from 0, see Figure 2c. Again $R(1, d, D)$ can also be studied analytically and one can find that the minimum is approximately 0.966.

Clearly, R is a continuous and bounded function of d_0, provided that $d_0 \geq \delta > 0$, so again the ratio R is bounded, and bounded away from zero in the region of interest. □

5.4 Discontinuity in the reconstruction cell

We now turn to point 4 of Summary 1. Let us consider the case in which the reconstruction is sought for the cell averages of a function with a discontinuity sitting inside the central cell. Clearly in this case all stencils of the polynomials involved in the reconstruction contain the troubled cell. Without loss of generality we restrict to the case in which $\overline{u}_j = 1$ for $j < 0$, $\overline{u}_0 = D \in (0, 1)$ and $\overline{u}_j = 0$ for $j > 0$.

We compute the CWENO reconstruction for $D \in [0, 1]$, $d_0 \in (0, 1]$ at a generic point x in the central cell. For CWENO 3 we choose the remaining coefficients symmetric, i.e. $d_L = d_R = (1 - d_0)/2$, as in Proposition 2. For CWENO 5 we have one more parameter and we take $d_L = d_R = d_C/2$, i.e. $d_C = (1-d_0)/2, d_L = d_R = (1-d_0)/4$. For CWENO 7 we again give more weight to the central stencils taking $d_L = d_R = (1-d_0)/3$ and $d_{LL} = d_{RR} = (1-d_0)/6$, see also (11).

We are thus left with the free parameters D and d_0 and applying the reconstruction we obtain a function $U(x; D, d_0)$. From these data, we fix d_0 and we extract $m_{d_0}(D) = \min_x U(x; D, d_0)$ and $M_{d_0}(D) = \max_x U(x; D, d_0)$. Figure 3 shows the plots of $m_{d_0}(D)$ and $M_{d_0}(D)$ for all schemes and for several values of d_0 which are typical, namely $d_0 = 0.5$ (often employed in the literature), $d_0 = 0.75$ (used in the numerical experiments of this paper), and $d_0 = 0.9$ (which overweights the central polynomial). It is clear that for all values considered, the reconstructed data are bounded by $[0, 1]$ for all values of D and thus no spurious oscillations are created and the total variation remains bounded.

It is noteworthy that the functions $m_{d_0}(D)$ and $M_{d_0}(D)$ depend so weakly on d_0. Moreover, we found comparable results for other choices of the coefficients in CWENO 5 and CWENO 7. Obviously, for d_0 close to 0 or 1, $m_{d_0}(D)$ and $M_{d_0}(D)$ would change significantly. However, taking extreme values for d_0 does not make sense in practice: for $d_0 \to 0$, P_0 becomes undefined, while the limit $d_0 \to 1$ leads to $P_{\mathsf{rec}} \to P_{\mathsf{opt}}$ irrespectively of the oscillation indicators.

6 Numerical experiments

The purpose of the tests appearing in this section is to study the accuracy of the reconstructions proposed in this work, and to verify the non oscillatory properties of the resulting schemes. Thus we will consider the standard tests which are

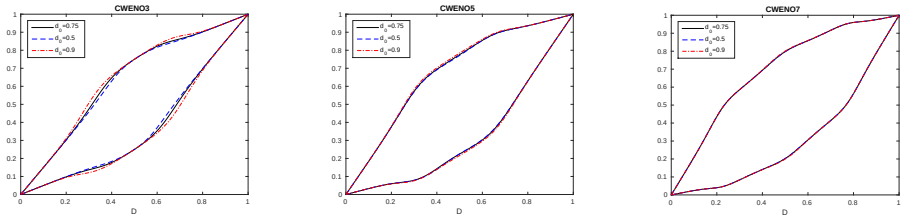

(a) (b) (c)

Figure 3: Discontinuity in the reconstruction cell. Minimum and maximum values attained by the reconstruction polynomial in the cell, as a function of the location D of the discontinuity, for several values of d_0. Left: CWENO 3 with $d_L = d_R = (1 - d_0)/2$. Middle: CWENO 5 with $d_C = (1 - d_0)/2, d_L = d_R = (1-d_0)/4$. Right: CWENO 7 with $d_L = d_R = (1-d_0)/3, d_{LL} = d_{RR} = (1-d_0)/6$.

commonly used in the literature on high order methods for conservation laws: linear advection of smooth and non smooth waves, shock formation in Burgers' equation and Riemann problems from gas dynamics. In all these cases, we will compare our results with solutions obtained with WENO schemes. Here, our results are comparable with standard WENO.

Next, we will consider problems with sources, where our reconstructions are, we think, an improvement over standard WENO, because we easily evaluate the reconstructions at all quadrature points simultaneously. Again, we exhibit convergence histories, and non oscillatory properties, using problems from shallow water and gas dynamics with source terms. Finally, we study the well balancing of the new reconstructions.

We construct numerical schemes applying the method of lines and the Local Lax-Friedrichs flux with the CWENO 3, CWENO 5 and the newly proposed CWENO 7 and CWENO 9 reconstructions. The time integrators are Runge-Kutta schemes of matching order. In particular, the third order scheme employs the classical third order (strong stability preserving) SSP Runge-Kutta with three stages [JS96], the fifth order scheme the fifth order scheme with six stages of [But08, §3.2.5], the scheme or order seven relies on the nine-stages scheme of [But08, pag 196] and the scheme of order nine employs the scheme with eighteen stages of order ten of [Cur75]. Clearly, multistep schemes and different Riemann solvers could be used as well.

Source terms are integrated with a Gaussian quadrature formula matching the order of the scheme when well-balancing is not an issue. In the case of the shallow water equations, we employ a scheme which is well-balanced for the lake at rest solution, constructed with the hydrostatic reconstruction technique of [ABB$^+$04], the desingularization procedure proposed in [KP07] and the Richardson extrapolation for the quadrature of the source term. With reference

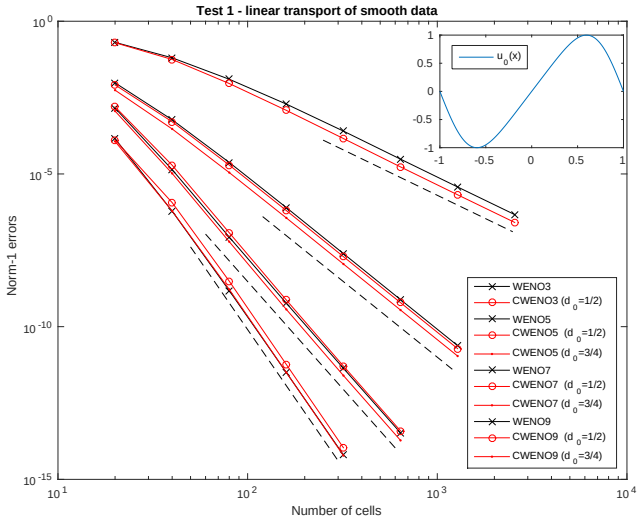

Figure 4: Convergence rates for CWENO and WENO schemes of order 3, 5, 7 and 9, Test 1.

to the latter, we employ the following quadratures $S^{(q)}$ of order q

$$
\begin{aligned}
S^{(4)} &= (4S_2 - S_1)/3 \\
S^{(6)} &= (64S_4 - 20S_2 + S_1)/45 \\
S^{(8)} &= (4096S_8 - 1344 * S_4 + 84S_2 - S_1)/2835 \\
S^{(10)} &= 1.450463049417298S_{16} - 0.481599059376837S_8 + 0.031604938271605S_4 \\
&\quad - 0.000470311581423S_2 + 0.000001383269357S_1,
\end{aligned}
$$

where S_n denotes the quadrature of the source term computed with the composite trapezoidal rule with n intervals on each cell. The first of these formulas was published in [NPPN06] and the othere ones were derived by us following the same ideas of that paper.

Test 1. *Linear transport of smooth data, low frequency case.*

The convergence rates appearing in Fig. 6 are obtained using an initial condition from[ABBM11]. We solve $u_t + u_x = 0$, on $[-1, 1]$ with periodic boundary conditions, up to $T = 2$, with initial condition

$$u_0(x) = \sin\left(\pi x - \frac{1}{\pi}\sin(\pi x)\right).$$

The low order CWENO3 scheme has $d_0 = \frac{1}{2}$, while for the higher order schemes we show results with $d_0 = \frac{1}{2}$ (empty circles) and $d_0 = \frac{3}{4}$ (dots). Each

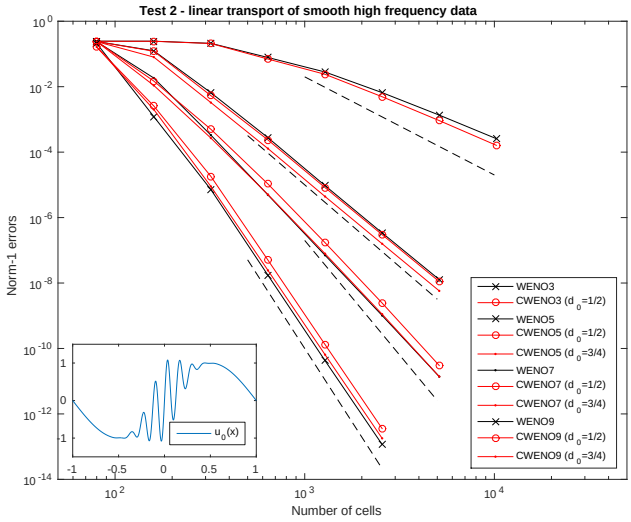

Figure 5: Convergence rates for CWENO and WENO schemes of order 3, 5, 7 and 9, Test 2.

group of curves is characterized with the desired slope (3, 5, 7 and 9 respectively, dashed black lines). The black solid curves are the reference results, obtained with the classical WENO scheme of the same order. Note that in all cases the errors almost coincide, with a very slight edge for the CWENO schemes with $d_0 = \frac{3}{4}$.

Test 2. *Linear transport of smooth data, high frequency case.*

This test is drawn from [SCR16]. It studies the propagation of a sine wave with a high frequency localized perturbation. As before, we solve $u_t + u_x = 0$, on $[-1, 1]$ with periodic boundary conditions, up to $T = 2$, but now the initial condition is

$$u_0(x) = \sin(\pi x) + \tfrac{1}{4}\sin(15\pi x)\, e^{-20x^2}.$$

Again, the correct rates are achieved in all cases. Note the high gain in accuracy obtained with the high order schemes even on coarse grids.

Test 3. *Burgers' equation: shock interaction*

This is a test on shock formation and shock interaction. We consider Burgers' equation in $[-1, 1]$ with initial condition

$$u_0(x) = 0.2 - \sin(\pi x) + \sin(2\pi x)$$

and periodic boundary conditions. The exact solution develops two shocks, which eventually collide, merging into a single discontinuity. We show three

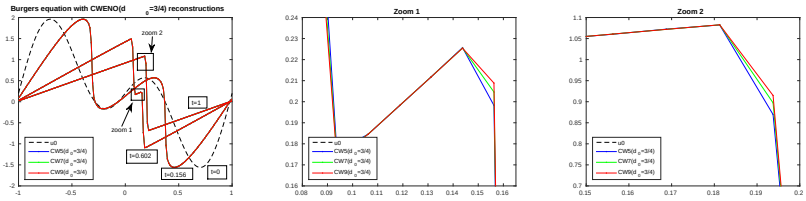

Figure 6: Burgers' equation and shock interaction: CWENO schemes. Evolution of the solution (left). Zoom slightly before (middle) and after (right) shock interaction.

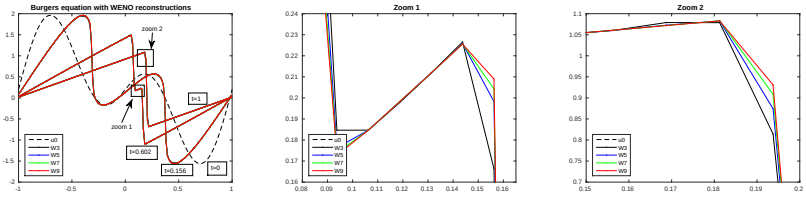

Figure 7: Burgers' equation and shock interaction: standard WENO schemes. Evolution of the solution (left). Zoom slightly before (middle) and after (right) shock interaction.

snapshots on the same panel in Figg. 6 and 7, with two zooms, which are enlarged on the right. The dashed black curve is the initial condition. The second curve is the solution at the time in which the two shocks develop ($T = 1/(2\pi)$). The third curve is slightly before shock interaction ($T = 0.6$), with a detail enlarged in the figure appearing in the center (zoom 1). The last curve is taken shortly after shock interaction ($T = 1$), and a zoom of the interaction region is shown in the right panel (zoom 2).

Fig. 6 shows the results obtained with CWENO schemes, with order 3, 5, 7, and 9 (black, blue, green and red curves respectively). The number of grid points is $N = 160$. It is clear that the schemes do not produce spurious oscillations, and have an excellent resolution of discontinuities. As the order is increased, the profiles become sharper. For comparison, we also show the same results, obtained with the WENO scheme in Fig. 7. Note that the results are very similar.

Test 4. *Gas dynamics: Lax' Riemann problem*

The equations of gas dynamics for an ideal gas in one space dimension are

$$\partial_t \begin{pmatrix} \rho \\ \rho u \\ E \end{pmatrix} + \partial_x \begin{pmatrix} \rho u \\ \rho u^2 + p \\ u(E+p) \end{pmatrix} = 0,$$

where ρ is the gas density, u the velocity, p the pressure, and E the energy per unit volume. The pressure is linked to the other variables through the

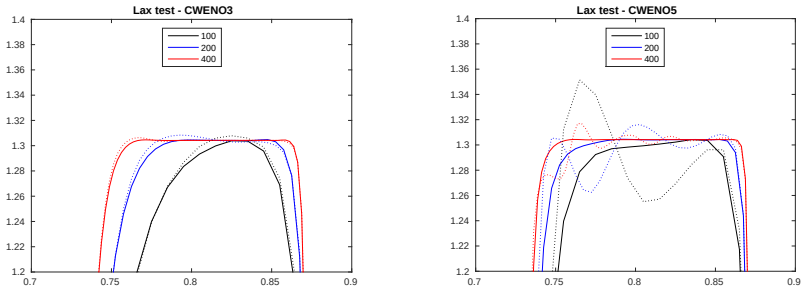

Figure 8: Lax' test. Zoom on the density peak. CWENO 3 (left) and CWENO 5 (right) on several grids. The reconstruction is computed along characteristic directions (continuous lines) and on conservative variables (dotted lines).

equation of state of an ideal gas, namely $p = (E - \frac{1}{2}\rho u^2)(\gamma - 1)$, and we take $\gamma = 1.4$. The Riemann problem by Lax has the following left and right states: $\rho_L = 0.445, u_L = 0.6989, p_L = 3.5277$ and $\rho_R = 0.5, u_R = 0, p_R = 0.571$. The solution develops a rarefaction wave travelling left, a contact discontinuity and a shock, with positive speeds. The most interesting region is the density peak which occurs between the contact and the shock wave, where high order essentially non oscillatory schemes are known to develop spurious oscillations. For this reason, we show only a zoom on the density peak. It is well known that essentially non oscillatory and WENO schemes develop oscillations with amplitude decreasing under grid refinement, while their amplitude increases with the order of the scheme, at a given mesh width.

The oscillations are originated by the interaction between waves in the first stages of the solution, when the discontinuities are so close that the algorithm cannot find a smooth stencil. Thus, they can be partly cured computing the reconstruction along characteristic fields, where the waves are approximately decoupled, [QS02].

Aggiungere la soluzione esatta nel density peak!

Fig. 8 contains the density peak obtained with CWENO3 (left) and CWENO5 (right) schemes. The continuous lines correspond to reconstructions computed along characteristic directions, for which the data in the whole stencil are projected along characteristic direction, before the reconstruction is computed, while the dashed curves are the standard reconstruction on conservative variables. Each figure contains the data obtained with $N = 100, 200$ and 400 grid points (black, blue and red curves, respectively). The improvement obtained with characteristic projection is quite dramatic, especially for the higher order schemes. In these two cases, the spurious oscillations disappear. Note also the improvement in the resolution of the waves with the high order CWENO5.

The following figure (Fig. 9) contains the results obtained with CWENO7 and CWENO9 (top row). As a comparison, the same results with the standard WENO 7 and WENO 9 schemes are included in the bottom row plots of the same

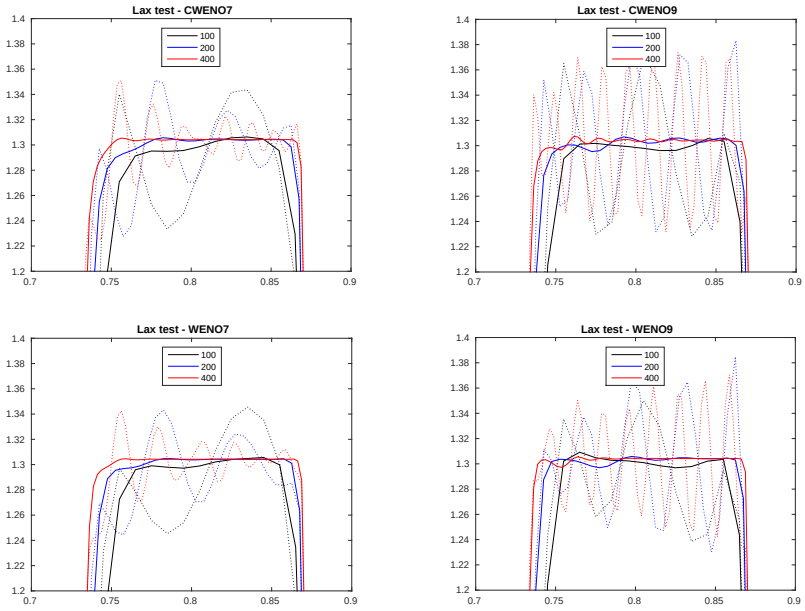

Figure 9: Lax' test. Zoom on the density peak. CWENO 7 (top left) and CWENO 9 (top right), WENO 7 (bottom left) and WENO 9 (bottom right) on several grids. The reconstruction is computed along characteristic directions (continuous lines) and on conservative variables (dotted lines).

figure. As expected, the spurious oscillations become wilder for these high order schemes, unless the reconstruction is computed along characteristic directions.

Aggiungere la soluzione esatta nel density peak!

The results discussed so far show that the new reconstructions are comparable to standard WENO reconstructions, not only as far as accuracy is concerned, but also in terms of non oscillatory, or essentially non oscillatory, properties. In both cases, for high order schemes, it is essential to employ characteristic projections, which could also be done in an adaptive way, as suggested in [Pup03] and[PS11].

We now turn to balance laws, where the new reconstructions permit to compute the cell averages of the source term with a single reconstruction.

Test 5. *Shallow water equations: convergence rates on a non-flat riverbed*

Now, we consider the shallow water system, namely

$$u = \begin{pmatrix} h \\ q \end{pmatrix} \qquad f(u) = \begin{pmatrix} q \\ q^2/h + \frac{1}{2}gh^2 \end{pmatrix} \qquad g(u,x) = \begin{pmatrix} 0 \\ -ghz_x \end{pmatrix}. \tag{37}$$

Here h denotes the water height, q is the discharge and $z(x)$ the bottom topography, while g is the gravitational constant.

	CWENO 3		CWENO 5		CWENO 7		CWENO 9	
N	error	rate	error	rate	error	rate	error	rate
16	4.62e-02		5.53e-03		1.34e-03		6.92e-04	
32	1.04e-02	2.16	4.13e-04	3.74	7.39e-05	4.18	2.83e-05	4.61
64	2.10e-03	2.30	1.75e-05	4.56	6.74e-07	6.78	1.23e-07	7.85
128	3.14e-04	2.74	5.78e-07	4.92	5.02e-09	7.07	3.45e-10	8.48
256	3.55e-05	3.15	1.82e-08	4.99	3.91e-11	7.00	7.44e-13	8.86
512	2.42e-06	3.88	5.71e-10	4.99	3.08e-13	6.99		

Table 2: Errors and convergence rates for SW convergence on a non flat riverbed.

Following [XS05], we compute the flow with initial data given by

$$z(x) = \sin^2(\pi x) \qquad h(0,x) = 5 + e^{\cos(2\pi x)} \quad q(0,x) = \sin(\cos(2\pi x)), \tag{38}$$

with periodic boundary conditions on the domain $[0,1]$. At time $t = 0.1$ the solution is still smooth and we compare the numerical results with a reference solution computed with the fourth order scheme and 16384 cells. The 1-norm of the errors appears in Table 2. The well balanced quadrature is computed using Richardson's extrapolation, based on the trapezoidal rule. This means that to achieve 5th order accuracy 3 points are needed per cell, while for 7-th and 9-th order accuracy 9 and 17 nodes respectively are used in each cell. We emphasise that all these reconstructed data are computed from a single CWENO reconstruction polynomial, using the same weights for all coefficients. Note that the order of accuracy is perfectly met, until machine precision is reached.

This test would be extremely demanding on a standard WENO reconstruction, since the non linear weights must be changed for each quadrature node.

Check the number of nodes of the quadrature formulas!! (I 3, 9 17 che ho scritto sopra!!

Test 6. *Shallow water equations: well-balancing test on a rough bottom*

This is a classical test, to explore the well balancing properties of a scheme, see [NPPN06]. We consider a flat lake $z(x) + h(x) \equiv 1.5$, with water at rest. The bottom cell averages are randomly extracted from a uniform distribution on $[0,1]$. Thus the function $z(x)$ is extremely irregular, but nonetheless the exact solution preserves the flat surface, and the water should remain still. A well balanced scheme preserves this solution at machine precision.

We report in Table 3 the values of the discharge computed by all CWENO schemes tested in this work for several grids. It is clear that in all cases the discharge is zero within machine precision, so that the quadrature of the source is indeed well balanced in all cases, notwithstanding the fact that, again, it is computed with a single polynomial for all quadrature nodes.

The data on the water height have the same precision, and are not reported for brevity.

Test 7. *Shallow water equation: dam-break*

method	error in q			
	N=100	N=200	N=400	N=800
CWENO 9	7.4471e-16	1.4354e-15	1.8279e-15	2.5115e-15
CWENO 7	2.1206e-15	3.0564e-15	7.1562e-15	1.6473e-14
CWENO 5	1.7490e-15	3.0874e-15	5.3284e-15	9.9496e-15
CWENO 3	1.9032e-15	3.5655e-15	4.7854e-15	7.6668e-15

Table 3: Well balancing errors on a rough lake at rest. Discharge

This test studies the movement of a shock and a rarefaction on a shallow water problem, with non constant bottom topography. The initial condition for the water surface $H(x) = h(x) + z(x)$ and the discharge is

$$H(x, t = 0) = \begin{cases} 1.5 & x < 0 \\ 0.5 & x > 0, \end{cases} \qquad q(x, t = 0) \equiv 0,$$

on $[-2, 2]$, and the bottom topography is $z(x) = 0.3\, e^{-10x^2}$. The final time is $t = 0.2$. This set up contains a discontinuity on the amount of water, in correspondance with a hump in the bottom topography. As the solution develops, a shock moves towards the right, while a rarefaction wave travels left.

The results on the water surface are shown in Fig. 10, with zooms on the most difficult parts of the solution for the CWENO 5, 7 and 9 schemes. Again, the numerical solution exhibits spurious oscillations behind the shock (red curve, with + markers), which can be levelled out using the characteristic projection, before evaluating the reconstruction (black solid lines). The same behaviour can be observed in the solution for the discharge.

Mancano i dati sulla griglia, qui e anche in altri posti. A proposito, la CFL è sempre la stessa? O ci sono dei miglioramenti usando RK via via più alti?

Test 8. *Gas dynamics: Riemann Problem in spherical cohordinates*

In the case of radial symmetry, the gas dynamics equations can be written as a 1D system, with a source term, which takes into account the geometrical effect, [Tor09, §1.6.3]. Radially symmetric solutions of the Euler equations in $\mathbb{R}^n$ may be computed by solving

$$\partial_t \begin{pmatrix} \rho \\ \rho u \\ E \end{pmatrix} + \partial_r \begin{pmatrix} \rho u \\ \rho u^2 + p \\ u(E + p) \end{pmatrix} = -\frac{n-1}{r} \begin{pmatrix} \rho u \\ \rho u^2 \\ up \end{pmatrix}.$$

We compute the so-called "explosion problem", which has a shock tube like initial data. In our case, we take the classical Sod's test, namely $(\rho_L, u_L, p_L) = (1, 0, 1)$ for $r < 0.5$ and $(\rho_R, u_R, p_R) = (0.125, 0, 0.1)$ for $r > 0.5$. The final time of the simulation is $t = 0.25$.

In order to avoid difficulties with the boundary conditions in the singular point $r = 0$, and taking into account that the computed solution will have null

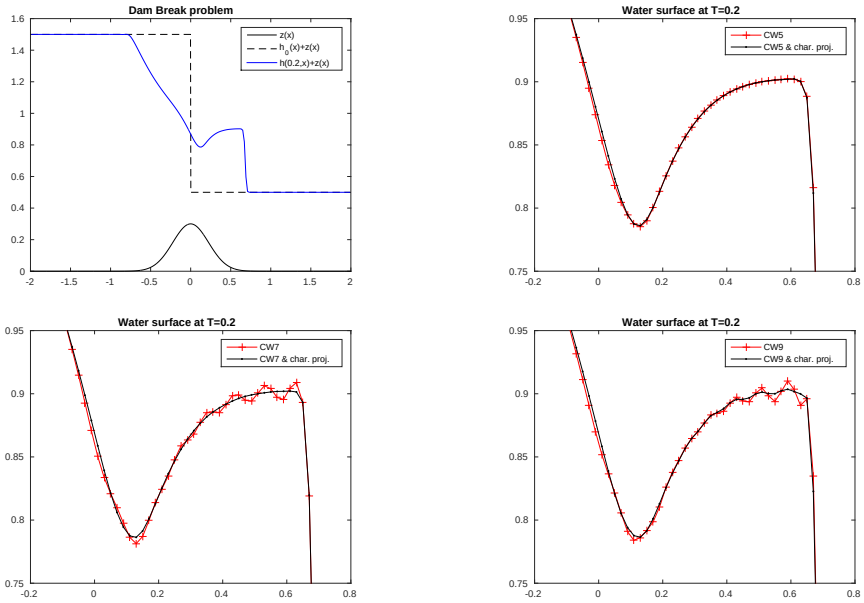

Figure 10: Dam break over a hump. Top left: water height at time $t = 0.2$. The remaining plots are zooms on the tail of the rarefaction and the jump, for CWENO $5, 7$ and 9. The black solid line is with characteristic projections.

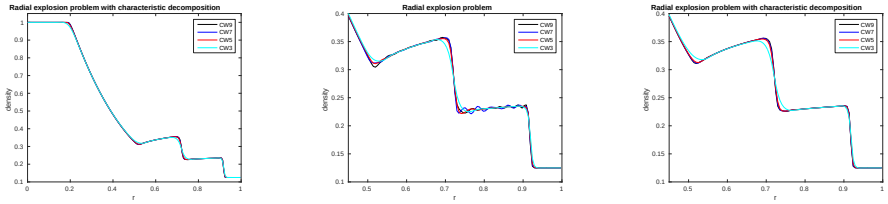

Figure 11: Sod's explosion problem: density profiles for several CWENO schemes (left), zoom on the contact and shock wave with the reconstruction computed along conservative variables (middle), and along characteristic variables (right).

velocity u (and thus null source term) close to $r = 0$, because of the initial data, we computed the solutions for $r \in [-1, 1]$ with symmetric initial data and free-flow boundary conditions. Gaussian quadrature formulas of appropriate order are employed to compute the cell average of the source term and the grid is chosen in order to avoid quadrature nodes at the singular point $x = 0$. The solution at final time is shown in the picture 11, restricted to the domain $r \in [0, 1]$. Again, we show the density profiles, since the density contains the main features of the flow. The zoom in the density profile centered on the contact wave is shown for the reconstruction computed along conservative variables (central plot of the figure), and along characteristic variables (right plot). Here too the dramatic improvement obtained with the projection along characteristic variables is striking. Each plot contains the solution obtained with all four different schemes tested in this work. The cyan curve is given by CWENO 3, and the improvement in the resolution of the contact wave obtained increasing the accuracy of the scheme is quite apparent. Here too, only one reconstruction polynomial is needed for each Runge Kutta stage.

7 Conclusions

In this paper we introduced a class of spatial reconstruction procedures that are charaterized by computing a reconstruction function whose accuracy is uniform across the whole cell, instead of reconstructed point values, as in the standard WENO reconstruction. This class of algorithms contains the already proposed CWENO 3 of [LPR99], CWENO 5 of [Cap08] and the two-dimensional third order reconstruction of [CRS16].

In particular, within this framework, we focused on one-dimensional reconstruction procedures of any odd order $2g+1$ (which were never considered before for $g > 2$) and proved that the nonlinear mechanism for stencil selection guarantees the desired accuracy of order $2g + 1$ when the procedure is applied to smooth enough data. The non-oscillatory properties of the reconstruction in the presence of discontinuities in the input data are studied more deeply than in previous papers and a sufficient condition (property R) is given, to direct the choice of the parameters appearing in the reconstruction, to avoid spurious

oscillations. Moreover, it is shown that the one-dimensional CWENO schemes studied in this paper satisfy property R, for orders up to 7 and under mild assumptions on the linear weights.

We think that this is the first time that the potential of these reconstructions is explored in the case of balance laws, and their properties are systematically studied.

The new schemes perform on par with WENO reconstructions regarding accuracy on smooth data and the production of spurious oscillations close to discontinuities, but they are, in our opinion, more versatile than WENO, because they result in a whole reconstructing polynomial which can be evaluated where needed. This is very important on balance laws, non uniform grids, moving mesh algorithms. In fact, in CWENO schemes, the accuracy requirements involve only the degree of the candidate polynomials and not the values of suitably chosen linear coefficients. This means that, in a CWENO procedure, the linear coefficients can be chosen independently of the point at which the reconstruction is to be evaluated and independently of the relative size of the neighbouring cells.

With these new schemes, unlike WENO, it is possible to compute boundary value reconstructions on uniform or non-uniform grids (to compute numerical fluxes), and, at the same time, evaluate the reconstruction at points in the interior of the computational cells, for evaluating quadratures of source terms, *with the same reconstruction polynomial*. The same polynomial can also be used to compute operations that employ quadrature formulas in the cell, as in the initialization of cell averages after a grid refinement on h-adaptive schemes or after mesh movement in moving mesh techiques. Another important application is the computation of cell averages of functions of the conserved variables arising in the computation of local residuals for a posteriori error control, as in the case of the numerical entropy error indicator. A very important application can be found in finite volume schemes for balance laws, in the computation of cell averages of source terms. This latter application in particular is tested in this paper, for accuracy orders up to 9.

In this paper we also introduce formulas to compute the reconstructions, in one space dimension, from the divided differences of the data in the case of non-uniform grids, and we provide tables of coefficients, obtained from undivided differences in the case of uniform grids. We note that the structure of these tables, whose entries do not depend on the degree of the polynomial to be computed, allows easily to raise or lower the degree of the reconstruction. The exploitation of this feature for p-adaptivity will be the subject for future work.

This paper is mainly concerned on CWENO reconstructions in 1D. The extension to multiD in the case of Cartesian grids is straightforward, but it is also possible to extend these techniques to unstructured grids.

References

[ABB+04] E. Audusse, F. Bouchut, M.O. Bristeau, R. Klein, and B. Perthame. A fast and stable well-balanced scheme with hydrostatic reconstruc-

tion for shallow water flows. *SIAM J. Sci. Comp.*, 25:2050–2065, 2004.

[ABBM11] F. Aràndiga, A. Baeza, A. M. Belda, and P. Mulet. Analysis of WENO schemes for full and global accuracy. *SIAM J. Numer. Anal.*, 49(2):893–915, 2011.

[But08] J. C. Butcher. *Numerical Methods for Ordinary Differential Equations*. Wiley, second edition, 2008.

[Cap08] G. Capdeville. A Central WENO scheme for solving hyperbolic conservation laws on non-uniform meshes. *J. Comput. Phys.*, 227:2977–3014, 2008.

[CFR06] E. Carlini, R. Ferretti, and G. Russo. A Weighted Essentially Non-Oscillatory large time-step scheme for Hamilton-Jacobi equations. *SIAM J. Sci. Comput.*, 27:1071–1091, 2006.

[CRS16] A. Coco, G. Russo, and M. Semplice. Adaptive mesh refinement for hyperbolic systems based on third-order Compact WENO reconstruction. *J. Sci. Comput.*, 66(2):692–724, 2016.

[CS] I. Cravero and M. Semplice. On the accuracy of WENO and CWENO reconstructions of third order on nonuniform meshes. *J. Sci. Comput.*

[Cur75] A. R. Curtis. High-order explicit Runge-Kutta formulae, their uses, and limitations. *IMA J. Appl. Math.*, 16(1):35–52, 1975.

[DB13] W.-S. Don and R. Borges. Accuracy of the Weighted Essentially Non-Oscillatory conservative finite difference schemes. *J. Comput. Phys.*, 250:347–372, 2013.

[DBTM08] M. Dumbser, D. S. Balsara, E. F. Toro, and C.-D. Munz. A unified framework for the construction of one-step finite volume and Discontinuous Galerkin schemes on unstructured meshes. *J. Comput. Phys.*, 227:8209–8253, 2008.

[DK07] M. Dumbser and M. Käser. Arbitrary high order non-oscillatory finite volume schemes on unstructured meshes for linear hyperbolic systems. *J. Comput. Phys.*, 221(2):693–723, 2007.

[FHW14] H. Feng, C. Huang, and R. Wang. An improved mapped Weighted Essentially Non-Oscillatory scheme. *Appl. Math. Comput.*, 232:453–468, 2014.

[Ger12] G.A. Gerolymos. Representation of the Lagrange reconstructing polynomial by combination of substencils. *Journal of Computational and Applied Mathematics*, 236:2763–2794, 2012.

[GITW12] Y. Gorsse, A. Iollo, H. Telib, and L. Weynans. A simple second order Cartesian scheme for compressible Euler flows. *J. Comp. Phys.*, 231(23), 2012.

[HAP05] A. K. Henrick, T. D. Aslam, and J. M. Powers. Mapped Weighted Essentially Non-Oscillatory schemes: Achieving optimal order near critical points. *J. Comput. Phys.*, 207:542–567, 2005.

[HOEC86] A. Harten, S. Osher, B. Engquist, and S. Chachravarty. Uniformly high order accurate Essentially Non-Oscillatory schemes III, 1986. NASA ICASE report 86-22.

[HS99] C. Hu and C.-W. Shu. Weighted Essentially Non-Oscillatory schemes on triangular meshes. *J. Comput. Phys.*, 150(1):97–127, 1999.

[JS96] G.-S. Jiang and C.-W. Shu. Efficient implementation of Weighted ENO schemes. *J. Comput. Phys.*, 126:202–228, 1996.

[Kol14] O. Kolb. On the full and global accuracy of a compact third order WENO scheme. *SIAM J. Numer. Anal.*, 52(5):2335–2355, 2014.

[KP07] A. Kurganov and G. Petrova. A second-order well-balanced positivity preserving central-upwind scheme for the Saint-Venant system. *Commun. Math. Sci.*, 5:133–160, 2007.

[KPL13] D. I. Ketcheson, M Parsani, and R. J. LeVeque. High-order Wave Propagation Algorithms for Hyperbolic Systems. *SIAM J. Sci. Comput.*, 35(1):351–377, 2013.

[LPR99] D. Levy, G. Puppo, and G. Russo. Central WENO schemes for hyperbolic systems of conservation laws. *M2AN Math. Model. Numer. Anal.*, 33(3):547–571, 1999.

[LPR00] D. Levy, G. Puppo, and G. Russo. Compact central WENO schemes for multidimensional conservation laws. *SIAM J. Sci. Comput.*, 22(2):656–672, 2000.

[NPPN06] S. Noelle, N. Pankratz, G. Puppo, and J. R. Natvig. Well-balanced finite volume schemes of arbitrary order of accuracy for shallow water flows. *J. Comput. Phys.*, 213(2):474499, 2006.

[PS11] G. Puppo and M. Semplice. Numerical entropy and adaptivity for finite volume schemes. *Commun. Comput. Phys.*, 10(5):1132–1160, 2011.

[PS14] G. Puppo and M. Semplice. Finite volume schemes on 2D non-uniform grids. In AIMS, editor, *Proceedings of "Fourteenth International Conference devoted to Theory, Numerics and Applications of Hyperbolic Problems" (HYP2012)*, 2014.

[PS16] G. Puppo and M. Semplice. Well-balanced high order 1D schemes on non-uniform grids and entropy residuals. *J. Sci. Comput.*, 2016.

[Pup04] G. Puppo. Numerical entropy production for central schemes. *SIAM J. Sci. Comput.*, 25(4):1382–1415 (electronic), 2003/04.

[Pup03] G. Puppo. Adaptive application of characteristic projection for central schemes. In Springer Verlag, editor, *Proceedings of "Hyperbolic Problems, Theory, Numerics, Applications"*, pages 819–829, 2003.

[QS02] J. Qiu and C.W. Shu. On the construction, comparison, and local characteristic decomposition for high-order central WENO schemes. *J. Comput. Phys.*, 183:187–209, 2002.

[SCR16] M. Semplice, A. Coco, and G. Russo. Adaptive mesh refinement for hyperbolic systems based on third-order compact WENO reconstruction. *J. Sci. Comput.*, 66:692–724, 2016.

[SHS02] J. Shi, C. Hu, and C.-W. Shu. A technique of treating negative weights in weno schemes. *J. Comput. Phys.*, 175(1):108–127, 2002.

[Shu98] C. W. Shu. Essentially Non-Oscillatory and Weighted Essentially Non-Oscillatory schemes for hyperbolic conservation laws. In *Advanced numerical approximation of nonlinear hyperbolic equations (Cetraro, 1997)*, volume 1697 of *Lecture Notes in Math.*, pages 325–432. Springer, Berlin, 1998.

[Shu09] C.-W. Shu. High order Weighted Essentially Non-Oscillatory schemes for convection dominated problems. *SIAM REVIEW*, 51(1):82–126, 2009.

[Tor09] E. F. Toro. *Riemann Solvers and Numerical Methods for Fluid Dynamics*. Springer, third edition, 2009.

[TT03] H. Tang and T. Tang. Adaptive mesh methods for one- and two-dimensional hyperbolic conservation laws. *SIAM J. Numer. Anal.*, 41(2):487–515, 2003.

[WFS08] R. Wang, H. Feng, and R. J. Spiteri. Observations on the fifth-order WENO method with non-uniform meshes. *Appl. Math. Comput.*, 196(1):433–447, 2008.

[XS05] Y. Xing and C. W. Shu. High order finite difference WENO schemes with the exact conservation property for the shallow water equations. *J. Comput. Phys.*, 208:206–227, 2005.